Biochimica et Biophysica Acta, 1017 (1990) 251–272
Elsevier

BBABIO 43214

Electrostatic control of charge separation in bacterial photosynthesis

William W. Parson [a], Zhen-Tao Chu [b] and Arieh Warshel [b]

[a] *Department of Biochemistry, University of Washington, Seattle, WA and* [b] *Department of Chemistry, University of Southern California, Los Angeles, CA (U.S.A.)*

(Received 3 October 1989)

Key words: Photosynthesis; Reaction center; Electron transfer; Charge separation; Electrostatics; Radical pair; Free energy

Electrostatic interaction energies of the electron carriers with their surroundings in a photosynthetic bacterial reaction center are calculated. The calculations are based on the detailed crystal structure of reaction centers from *Rhodopseudomonas viridis*, and use an iterative, self-consistent procedure to evaluate the effects of induced dipoles in the protein and the surrounding membrane. To obtain the free energies of radical-pair states, the calculated electrostatic interaction energies are combined with the experimentally measured midpoint redox potentials of the electron carriers and of bacteriochlorophyll (BChl) and bacteriopheophytin (BPh) in vitro. The $P^+H_L^-$ radical-pair, in which an electron has moved from the primary electron donor (P) to a BPh on the 'L' side of the reaction center (H_L), is found to lie approx. 2.0 kcal/mol below the lowest excited singlet state (P*), when the radical-pair is formed in the static crystallographic structure. The reorganization energy for the subsequent relaxation of $P^+H_L^-$ is calculated to be 5.0 kcal/mol, so that the relaxed radical-pair lies about 7 kcal/mol below P*. The unrelaxed $P^+B_L^-$ radical-pair, in which the electron acceptor is the accessory BChl located between P and H_L, appears to be essentially isoenergetic with P*. $P^+B_M^-$, in which an electron moves to the BChl on the 'M' side, is calculated to lie about 5.5 kcal/mol above P*. These results have an estimated error range of ±2.5 kcal/mol. They are shown to be relatively insensitive to various details of the model, including the charge distribution in P^+, the atomic charges used for the amino acid residues, the boundaries of the structural region that is considered microscopically and the treatments of the histidyl ligands of P and of potentially ionizable amino acids. The calculated free energies are consistent with rapid electron transfer from P* to H_L by way of B_L, and with a much slower electron transfer to the pigments on the M side. Tyrosine M208 appears to play a particularly important role in lowering the energy of $P^+B_L^-$. Electrostatic interactions with the protein favor localization of the positive charge of P^+ on P_M, one of the two BChl molecules that make up the electron donor.

Introduction

The elucidation of the crystal structure of purple bacterial reaction centers [1–5] has raised the challenge of relating the energetics and kinetics of the photosynthetic electron transfer reactions to the structure of the protein. One of the key problems is to reconcile the specificity of the initial electron transfer steps with the symmetry of the structure. The reaction center contains a bacteriochlorophyll (BChl) dimer that serves as the primary electron donor (P), two 'accessory' BChls (B_L and B_M), two bacteriopheophytins (BPh, H_L and H_M) and two quinones (Q_A and Q_B). The electron carriers are arranged as shown in Fig. 1, in two, nearly symmetrical branches on two subunits of the protein. B_L, H_L, Q_B and one of the BChls of P are surrounded predominantly by residues of subunit L; B_M, H_M, Q_A and the other BChl of P, by residues of subunit M. About a quarter of the corresponding amino acid residues in the two polypeptides are identical, and many others represent conservative replacements [6–10]. Despite this symmetry, the primary charge-separation process occurs almost exclusively along the L branch of the pigments [11–16]. When the reaction center absorbs a photon, an electron moves from the excited BChl dimer (P*) to H_L with a time constant of about 3 ps [17–23]. The radical anion H_L^- then reduces Q_A in about 200 ps. Although H_M also can undergo photoreduction under special conditions [24], this process has a much lower quantum

Abbreviations: BChl, bacteriochlorophyll; BPh, bacteriopheophytin; PDLD, protein dipoles, Langevin dipoles; QCFF/PI, quantum consistent force field for π electrons.

Correspondence: W.W. Parson, Department of Biochemistry SJ-70, University of Washington, Seattle, WA 98195, U.S.A.

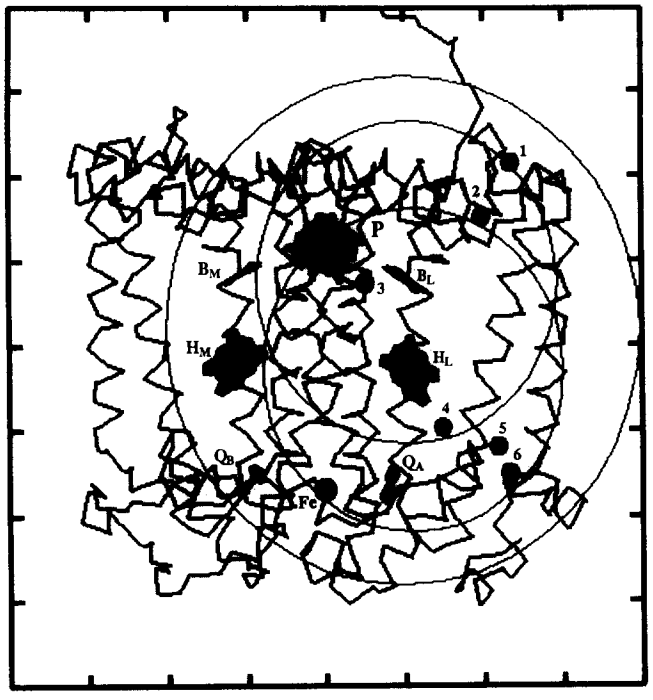

Fig. 1. Pigments and C_α carbon chains of the L and M subunits of the reaction center of *Rp. viridis*. The L subunit is on the right. BChls, BPhs, quinones and the Fe are indicated with solid shading. (The phytyl side-chains are not shown.) The tics on the frame represent 10-Å intervals. The circles with radii of 19 Å centered on B_L and H_L indicate regions of the X-ray structure that were treated explicitly in the electrostatic calculations on the reaction $P^+B_L^- \rightarrow P^+B_LH_L^-$; all amino acid residues with one or more atoms inside either of these spherical regions were included in the model. (Residues of the cytochrome and H subunits, which are not shown in the Fig., also were included.) The 30-Å circle indicates the region was filled by adding polarizable atoms on a cubic grid. Calculations also were done with structures obtained by using cutoff radii of 17 Å. The six filled circles with 1-Å radii indicate the positions of Tyr-M208 and Glu-L104, and of ionizable amino acid residues that probably make small contributions to ΔG for the reaction $P^+B_L^-H_L \rightarrow P^+B_LH_L^-$. These circles are centered on (1) C_ζ of Arg-C15, (2) C_γ of Asp-L60, (3) the phenolic O of Tyr-M208, (4) $O_{\varepsilon 1}$ of Glu-L104, (5) C_ζ of Arg-L103 and (6) C_δ of Glu-L106.

yield and does not ordinarily compete significantly with electron transfer to H_L. The specificity of the pathway to H_L offers an opportunity for probing the control of electron transfer pathways by protein microenvironments, and could provide a critical test case for theoretical methods of structure-function correlations in proteins.

Because B_L is located between P and H_L (Fig. 1), it seems likely to play an important role in the initial electron transfer reaction. The exact nature of this role is still unclear. One possibility is that an initial transfer of an electron from P* to B_L creates an intermediate radical-pair, $P^+B_L^-$, which then passes an electron to H_L. Alternatively, the reaction could occur by a 'superexchange' mechanism in which $P^+B_L^-$ mixes quantum mechanically with P* and with $P^+H_L^-$ but does not form as a discrete intermediate. Although there have been indications of the possible formation of $P^+B_L^-$ as an intermediate [25,26], most of the recent attempts to detect this state in time-resolved absorbance measurements have given negative results [17–23,27–29]. Holzapfel et al. [30] have obtained evidence for an intermediate species that decays with a time constant of 0.9 ps, and have suggested that this is $P^+B_L^-$, but they have not yet presented a full characterization of this species.

The electron-transfer mechanisms that have been suggested differ in their dependence on the free energies of the radical-pair states. The formation of $P^+B_L^-$ as a discrete intermediate could occur rapidly only if the intermediate radical-pair lies close to or below P* in energy. Thus, the specificity of the initial electron-transfer reaction could be explained straightforwardly if $P^+B_L^-$ has a lower energy than P*, while $P^*B_M^-$ has a substantially higher energy. The superexchange mechanism could operate even if the $P^+B_L^-$ radical-pair lies above P*, but the mixing of the two states will decrease as the states move apart in energy [16,31,32]. A difference in energy between $P^+B_L^-$ and $P^+B_M^-$ thus could explain the reaction specificity by the superexchange mechanism also, although the difference might have to be larger than that required in a two-step mechanism.

Estimates of the free energy of $P^+H_L^-$ have been obtained by studying the metastable radical-pair that is formed on illumination when electron transfer from H_L^- to Q_A is blocked. This state (P^+I^-, or P^F) lives for about 15 ns before it decays by back-reactions from I^- to Q_A [11,33,34]. The very weak exchange interaction between the two radicals (P^+ and I^-) implies that the oxidized and reduced species are relatively far apart [35,36], which is consistent with the identification of I^- as H_L^-. The delayed fluorescence from P* during the lifetime of P^+I^- provides a measure of the effective equilibrium constant between the excited state and the radical-pair. Such measurements suggest that, in *Rhodobacter sphaeroides* reaction centers at 295 K, P^+I^- initially is located about 0.17 eV (3.9 kcal/mol) below P*, but that the radical-pair undergoes relaxations that increase this free energy gap to the range of 0.25 eV (5.8 kcal/mol) on the time scale of several nanoseconds [37–39]. The free energy of the relaxed radical-pair also has been estimated by analyzing the decay kinetics of a triplet state of P (^3P) that forms by way of P^+I^- [34,40–42]. Because ^3P decays partly by returning to P^+I^-, the temperature dependence of the decay kinetics provides information on the enthalpy difference between these two states. This in turn yields the enthalpy of P^+I^- because ^3P is known to lie 0.40 eV below P*. The studies of ^3P agree with the measurements of delayed fluorescence that the free energy difference (ΔG) between P* and the relaxed form of P^+I^- at moderate temperatures is about 0.25 eV, but the two measure-

ments appear to disagree at cryogenic temperatures. The decay kinetics of ^3P suggest that ΔG is primarily enthalpic in nature and does not vary greatly with temperature [34,40–42]. The temperature dependence of the delayed fluorescence suggests that ΔG includes a substantial entropy change and decreases with decreasing temperature [37]. This discrepancy remains to be resolved, but could reflect the use of different techniques to block electron transfer between H_L^- and Q_A.

At present, there is no direct experimental information on the energy of $P^+B_L^-$. However, Bixon et al. [43] have estimated that, in *Rb. sphaeroides*, $P^+B_L^-$ must lie above $P^+H_L^-$ by at least 5 kcal/mol. This estimate pertains to reaction centers in which electron transfer is blocked, so that P^+I^- has several nanoseconds to relax after the initial charge separation. Bixon et al. pointed out that the exchange interaction between P^+ and I^- appears to be essentially independent of temperature [44,45]. Because B_L^- would be expected to interact with P^+ much more strongly than H_L^- does, the effective exchange interaction should increase with temperature if I^- contained an appreciable amount of B_L^- in equilibrium with H_L^-. The insensitivity of the exchange interaction to temperature thus allows one to put a lower limit on the enthalpy difference between the two states, but does not provide an upper limit.

In recent work [31,46], we have described preliminary simulations of the energetics and dynamics of the initial electron transfer steps in bacterial reaction centers. The free energies of the radical-pair states were calculated by a microscopic approach that combined the crystallographic structural information with experimental information on the midpoint redox potentials of P and of BChl and BPh in solution. As a model system, we also have calculated the energies of radical-pair states of crystalline methylbacteriopheophorbide [47]. In the latter case, the calculated energies agreed well with the spectroscopic properties of the crystal. Although the calculations on the reaction center appeared to favor the two-step electron transfer pathway through $P^+B_L^-$ [31], these studies were not able to discriminate unambiguously between the superexchange and two-step mechanisms because the free energies of the radical-pair states could not be calculated to the necessary accuracy. The calculated free-energies had an error range of ± 5 kcal/mol. In the present work, we have carried out a more extensive series of calculations with the aim of reducing this uncertainty and of exploring how various features of the structure contribute to the energies. To obtain an improved estimate of the energy of $P^+B_L^-$, we have emphasized calculations of the energetics of charge transfer processes such as $P^+B_L^-H_L \rightarrow P^+B_LH_L^-$, because these are expected to have a smaller error range than calculations of charge separation processes such as $P^*B_L \rightarrow P^+B_L^-$. We also have focused on the differences between the energetics on the L and M branches of the reaction center, because calculations of the energy differences between radical-pairs on the two branches should be more reliable than calculations of the absolute values of the energies.

Methods

The PDLD (protein dipoles, Langevin dipoles) method, which has been used previously for electrostatic calculations in other proteins [48–53] and in crystalline methylbacteriopheophorbide [47], provides a relatively straightforward way of evaluating the energy of a radical-pair state such as $P^+H_L^-$. In this approach, one takes the X-ray crystallographic coordinates at face value and calculates the electrostatic energy in the average protein structure as an approximation of the average of the energy over the protein configurations. The standard, partial-molecular free energy change in an electron-transfer reaction is expressed as

$$\Delta G = \alpha + \Delta G_{\text{elec}} \tag{1}$$

where α is the energy of the gas-phae reaction when the electron donor and acceptor are infinitely far apart, and ΔG_{elec} is the total change in the free energy of electrostatic interactions of the two electron carriers with each other and with their surroundings in the protein.

The electrostatic free energy difference in Eqn. 1 can be broken into five parts:

$$\Delta G_{\text{elec}} = \Delta V_{\text{QQ}} + \Delta V_{\text{Q}\mu} + \Delta V_{\text{ind}} + \Delta G_{\text{H}_2\text{O}} + \Delta G_{\text{bulk}} \tag{2}$$

Here ΔV_{QQ} represents the change in the energy of interactions between the charges on the two electron carriers; $\Delta V_{\text{Q}\mu}$ is the change in the interaction of the charges on the electron carriers with the charges of the protein atoms and the other prosthetic groups of the reaction center; ΔV_{ind} is the change in interaction with induced dipoles that result from the polarizabilities of the other atoms; $\Delta G_{\text{H}_2\text{O}}$ represents the change in interactions with water or other solvent molecules in the structure; and ΔG_{bulk} is the change in interaction of the surrounding bulk solution with the atoms in the region of the structure that is treated microscopically.

The charge–charge interaction energies in Eqn. 2 are given (in kcal/mol) by

$$V_{\text{QQ}} = 332 \sum_i \sum_j Q_i Q_j / r_{ij} \tag{3}$$

where Q_i and Q_j are the charges on atom i of the electron donor and atom j of the acceptor, and the interatomic distances (r_{ij}) are in Å [48]. The charges on atoms that are part of the π system of BChl or BPh were obtained with the QCFF/PI procedure [47,51,54]; the charges on other atoms of the electron carriers were assigned essentially as described by Russell and Warshel

[49] for amino acid sidechains. A listing of the atomic charges for BChl and BPh is given in the Appendix. For most of the calculations involving P^+, the net positive charge on the BChl dimer was divided equally between molecules P_L and P_M, but the effects of varying the charge distribution were also examined.

The second term on the right in Eqn. 2 is given by

$$V_{Q\mu} = 332 \sum_i \sum_s Q_i q_s / r_{is} \quad (4)$$

where index i is taken over the atoms of both electron carriers, and the q_s values are the residual charges on the surrounding atoms of the system. In most of the calculations presented below, the system that was treated microscopically in this way included all of the amino acid residues in the *Rp. viridis* crystal structure [3] that had one or more atoms within 17 Å of either the center of the electron donor or the center of the electron acceptor. Residues of the cytochrome polypeptide were included along with those of the L, M and H subunits if they were within the prescribed region. The system also included the four BChls and two BPhs (with the entire phytol side chains) the carotenoid, the head groups and first two prenyl units of the side-chains of both quinones (menaquinone and ubiquinone) and the two water molecules that are close to P, B_L and B_M in the X-ray structure [3]. This typically amounted to between 3800 and 4500 atoms, depending on the electron-transfer reaction under consideration. To determine whether the model included a sufficiently large region of the protein, calculations also were done with structures defined by cutoff distances of 19 Å instead of 17 Å (Fig. 1).

The crystallographic coordinates used in the calculations have been refined at 2.3 Å resolution [3]; they are available from the Brookhaven Data Bank. Hydrogen atoms were added to the X-ray structure by standard procedures. Glutamic acid L104, Thr-L248, Tyr-M195, and the two waters were assumed to be hydrogen-bonded to the pigments as described by Michel et al. [2,3]. The phenolic hydrogen of Tyr-M208 was rotated about the C_ζ–O bond to minimize the energy of electrostatic interactions with the neighboring residues when all of the electron carriers were in their resting states. Most of the electrostatic calculations were done with the phenolic hydrogen fixed in this optimal position, but calculations also were done with rotation angles of $\pm 40°$ on either side of the optimum.

The atomic charges assigned to the amino acid residues were as described by Russell and Warshel [49] for most amino acids, and as given by Warshel and Russell [50] for the side-chains of histidine, aspartatic acid and glutamic acid. For comparison, we also carried out calculations using the atomic charges of the AMBER force field [55], with minor adjustments to make each residue electrically neutral overall. Except where specified otherwise, all potentially ionizable amino acid residues were taken to be in their neutral forms, and the nonheme Fe atom was given a charge of zero. The effects of the charges on these atoms will be considered in more detail below.

The sum over s in Eqn. 4 is taken over all of the protein and pigment atoms in the region that is treated microscopically, with the exclusion of the electron donor and acceptor. The phytol side chains of the BChls and BPhs were included in the surroundings, rather than being treated as parts of the electron carriers. Histidines L153, L173, M180 and M200, which act as axial ligands to B_L, B_M and the two BChls of P, were treated in two different ways. In 'treatment 1', when the electron transfer reaction of interest involved one of the BChls, the imidazole ring of the attached histidine was considered to be part of the electron carrier. In 'treatment 2', the imidazole ring was considered to be part of the surrounding protein. Thus, in treatment 1 the atoms of the imidazole ring were included in the sum over i in Eqn. 4 and in the sum over i or j in Eqn. 3; in treatment 2, they were included in the sum over s in Eqn. 4. The results of both treatments will be presented in parallel below.

The third term on the right in Eqn. 2, which describes interactions with induced dipoles in the surroundings, can be written

$$V_{\text{ind}} = 166 \sum_s \kappa_s (\xi_s)^2 \quad (5)$$

where κ_s is the polarizability of atom s (in $Å^3$) and ξ_s is the field on this atom from all the other atoms in the system (in atomic charges/$Å^3$). The field was evaluated by an iterative, self-consistent procedure, using a polarizability of 0.5 $Å^3$ for H atoms and 1.0 $Å^3$ for other atom [48,49]. Setting κ_s to zero for H atoms and 1.2 $Å^3$ for other atoms gave similar results.

To simulate the effects of more distant parts of the protein and the membrane or detergent surrounding the protein, the portion of the X-ray structure described above was completed to a sphere with a radius of 30 Å by adding uncharged, but polarizable atoms at points on a cubic grid with a 4 Å spacing (Fig. 1). Grid points that were within Van der Waals contact distance of a crystallographic atom were omitted. The atoms added on the grid were included with the crystallographic atoms in the sum over s in Eqn. 5. The polarizability assigned to the atom added at a particular grid point was determined by whether the point would be inside or outside of the hydrophobic region of the phospholipid bilayer. The hydrophobic region was taken to be the space between two planes perpendicular to the reaction center's axis of local rotational symmetry, which were positioned 40 Å apart near the edges of the transmem-

brane α-helices. (Yeates et al. [56] have identified the hydrophobic region by an energy-minimization procedure based on the polarity of the amino acid side chains. Neutron diffraction studies have shown that in the isolated reaction center this region is surrounded by a belt of detergent molecules [83].) The polarizabilities were chosen so as to give the grid atoms a bulk dielectric constant of 2.0 inside the hydrophobic region and 4.0 outside. For this purpose, the dielectric constant (ε) was related to the polarizability (κ) and the atomic density of the grid (ρ) with the Clausius-Mosotti equation [48]:

$$(\varepsilon-1)/(\varepsilon+2) = 4\pi\rho\kappa/3 \tag{6}$$

A dielectric constant of 4 rather than 80 was used for the outer region because this part of the crystal structure is occupied mainly by the cytochrome and H polypeptides rather than by water. This choice had little effect on the results.

For each electron-transfer reaction that was considered, we generated between 20 and 40 different grids centered at random points near the geometric center of the electron donor and acceptor, and selected the grid that resulted in the largest interactions with the donor and acceptor. (Taking a Boltzmann average of the energies over all the grids would lead to similar results.) The number of atoms added on the grid was typically about 1200, bringing the total number of atoms in the model to between 5000 and 5800, or up to about 6550 when the cutoff distance for including amino acid residues was increased to 19 Å. The total contribution of the grid atoms to ΔV_{ind} was typically about 0.8 kcal/mol. Alternative choices of the grid center or the bulk dielectric constants had little effect on the results because most of the atoms that were added were more than 15 Å from the electron carriers. Using Langevin dipoles [48,49] to simulate water at the grid points outside the hydrophobic region also gave similar results.

The PDLD program ordinarily evaluates ΔG_{H_2O} by modeling the water with a cubic grid of Langevin dipoles [48,49]. This was not done in most of the calculations described here, because there is relatively little water in the parts of the structure that were treated microscopically. Instead, the two molecules of bound water that are located near the pigments [3] were included explicitly in Eqns. 4 and 5 as described above. The other molecules of bound water seen in the X-ray structure [3] are far enough from the electron carriers so that their effects on the free energy changes probably are negligible. The effects of some of these water molecules, and of other, more loosely bound water, were represented in an approximate manner by the polarizable atoms that were added to complete the structure to a sphere.

The final term in Eqn. 2 can be evaluated with the expression [48]:

$$G_{bulk} = -166[(Q^2/b)(1-1/\varepsilon)+(2|\mu|^2/b^3)(\varepsilon-1)/(2\varepsilon+1)] \tag{7}$$

Here b is the radius of the spherical region that is treated microscopically (including the grid atoms that model the membrane); Q is the total charge inside this sphere; ε is the dielectric constant of the bulk solution outside the sphere; and $\mu = \Sigma_t q_t \mathbf{r}_t$, where q_t and $\mathbf{r}_t$ are the charge of atom t and the vector from the center of the sphere to that atom. The sum includes contributions from the protein and the other pigments, in addition to the electron carriers that are involved in the electron transfer reaction. If the system has no net charge, or if the center of charge coincides with the center of the sphere, μ reduces to the dipole moment. We used a value of 80 for ε, but decreasing this to 2 had relatively small effects on the calculated values of ΔG_{elec} because in most cases ΔG_{bulk} made only small contributions to the free energy changes.

The version of PDLD used to calculate ΔV_{elec} for the reaction center was an adaptation of the program POLARIS [53]. A calculation typically required between 6 and 10 h on a MicroVAX II computer, depending on the number of atoms in the model. Most of this time was devoted to the iterative evaluation of ΔV_{ind}, which took 5 or 6 iterations to converge.

The gas-phase energy differences in Eqn. 1 were estimated by combining the midpoint redox potentials (E_m values) of the electron carriers with calculated solvation energies for the oxidized and reduced carriers [31,47]:

$$\alpha = \Delta G^w_\infty - \sum \Delta G^w_{sol} \tag{8}$$

$$\Delta G^w_\infty = -nF[E^A_m - E^D_m] \tag{9}$$

where $n = 1$ electron/molecule, F is the Faraday constant, E^A_m and E^D_m are the E_m values of the electron acceptor and donor, and $\Sigma\Delta G^w_{sol}$ is the sum of the solvation energies for the individual radicals, relative to the solvation energies of the neutral molecules. The redox potentials for the oxidation of P and for the reduction of H_L have been measured in the reaction center itself [57–61]. The solvation free energies for the individual radicals in the protein can be calculated as outlined above for the electrostatic free energies of radical-pairs. However, these calculations are based on the static X-ray structure and do not take into account structural relaxations that occur after the formation of the oxidized or reduced species. The measured redox potentials pertain to fully relaxed species. The solvation energy ΔG^w_{sol} for each radical, therefore, must include a reorganization energy, λ, in addition to the electrostatic energy calculated with the static structure (Fig. 2). The reorganization energies associated with the formation of

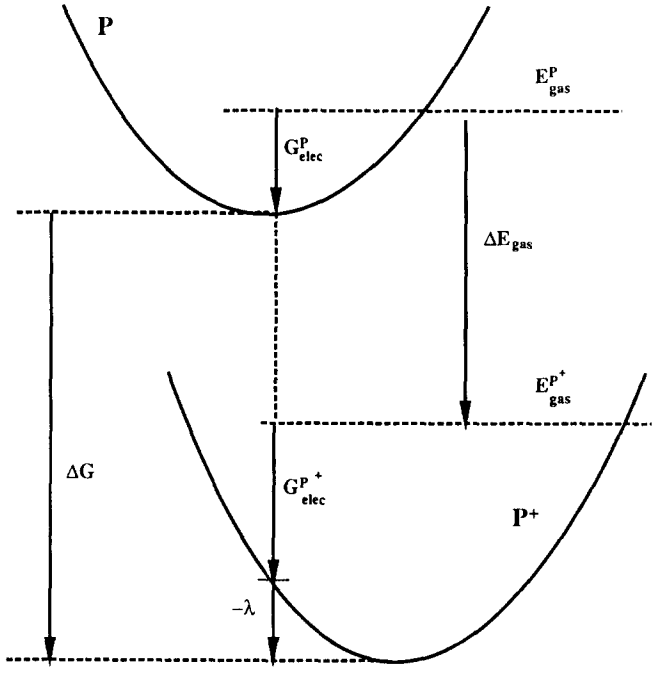

Fig. 2. Schematic drawing of the changes in electrostatic energies and partial molecular free energies associated with the oxidation of P. The parabolas represent the potential energy surfaces of P and P^+ as functions of the protein coordiantes. The electrostatic free energies of P and P^+ (G^{P}_{elec} and G^{P+}_{elec}) are calculated using the static X-ray structure, which reflects the geometry of the system when P is in the unoxidized state. The change in free energy accompanying the relaxation of the oxidized system to its equilibrium geometry is $-\lambda$. The solvation free energy of P is simply G^{P}_{elec}; that of P^+ is the sum of G^{P+}_{elec} and $-\lambda$. E^{P}_{gas} and E^{P+}_{gas} represent the gas-phase energies of P and P^+. The change in standard partial molecular free energy (ΔG) associated with the oxidation of P is given by $\Delta E_{gas} + \Delta G_{elec} - \lambda$. In a complete electron-transfer reaction, the gas-phase energy difference (α) is the sum of ΔE_{gas} for the electron donor and acceptor, and the overall ΔG and λ consist of similar sums. (If the potential energy surfaces for the reactants and products have the same curvature, the activation energy for bringing the reactants to the transition state for the electron transfer reaction is given by $(\lambda + \Delta G)^2/4\lambda$.)

P^+ and H_L^- were calculated by a free-energy-perturbation method [31,51,62], in which molecular dynamics simulations were carried out while the net charge on the electron carrier was changed gradually from 0 to ± 1. These calculations were done on an alliant minisupercomptuer using the program ENZYMIX [53]. The structures used in the simulations included all amino acid residues with one or more atoms within 18 Å of the center of the electron carrier. Molecules of water were added as needed to fill empty spaces in the structure.

Because the E_m for reduction of B_L has not been measured in the reaction center, the application of Eqns. 8 and 9 to the reaction $B_L^- H_L \rightarrow B_L H_L^-$ requires the use of E_m values for BChl and BPh measured [63–65] in polar organic solvents. Solvation free energies for the radicals in vitro can be calculated with the PDLD method [48,49], using a grid of Langevin dipoles to model the solvent. For these calculations, we used the geometry of B_L and H_L, but truncated the phytol side-chains after the first methylene group to remove any dependence of the results on the particular geometries of the side-chains in the reaction center. (The solvation energy for BChl or BPh in solution represents an average over many conformations of the side-chain. In calculating the free energy difference between $P^+B_L^-$ and $P^+H_L^-$ we are concerned only with the difference between the solvation free energies for $BChl^-$ and BPh^-, so the absolute magnitude of the average solvation free energies contributed by the side chains are relatively unimportant as long as they are approximately the same for the two molecules.) Because the E_m value for the reduction of BChl was measured in butyronitrile [63], we replaced the histidyl axial ligand of B_L by a nitrile ligand, acetonitrile. (The Mg atom of BChl is 5-coordinate in acetonitrile, having a molecule of acetonitrile as its axial ligand [84]; the coordination state should be the same in butyronitrile.) Separate calculations were done with the acetonitrile treated either as part of the BChl (treatment 1), or as part of the solvent (treatment 2). Calculations also were done with a series of structures in which the distance between the Mg and the acetonitrile N was varied from 1.9 to 2.4 Å, but this variation had little effect on the final values of $\Sigma\Delta G^{w}_{sol}$ ($< \pm 0.5$ kcal/mol). The numbers presented below are for a Mg–N distance of 2.2 Å, a grid radius of 17 Å and a grid spacing of 1.8 Å. Separate calculations of the reorganization energies are not needed here, because the Langevin procedure models a fully relaxed solvent.

Although the PDLD method was parametrized originally for ionization reactions in water [48,49], no special modifications beyond the attention to BChl's axial ligand should be needed in order to apply the method to another polar solvent such as butyronitrile or dimethylformamide. Changes in solvation energies associated with going from one polar solvent to another are known to be very small [48]. This is in accord with the Born Eqn. (Eqn. 7), which is insensitive to ε for any ε greater than about 30. In a previous study [47], a PDLD treatment of methylbacteriopheophorbide radicals appeared to give somewhat larger solvation energies than a free-energy perturbation method based on an all-atoms model of the solvent, but the discrepancy probably was due to incomplete convergence in the implementation of the Langevin algorithm. In the present work we found that the two treatments agreed to within 2 kcal/mol, provided that the evaluation of the Langevin dipoles was continued for a sufficiently large number of iterations and that the cutoff distance for including dipole–dipole interactions was sufficiently long. The program

used here first employed a noniterative routine to examine 25 different grids centered at random points near the geometric center of the radical, and then carried out 50 iterations of the Langevin algorithm [48,49] with the grid that gave the largest solvation energy. This was done five times for each radical of interest and the results obtained with the five different grids were averaged.

Electrostatic energies for the ionization of amino acid side-chains in the reaction center and in solution were calculated using the PDLD procedure essentially as outlined above for the electron carriers, except that a grid of Langevin dipoles was used instead of the membrane model to complete the microscopic system. For the calculations on the protein, the regions that were treated microscopically included all of the amino acid residues that had one or more atoms within 15 Å of the ionizable group.

The interaction matrix element that mixes the $|P_L^+\rangle$ and $|P_M^+\rangle$ basis states (U_{LM}) was calculated as described previously [47,66–68], using the refined crystallographic coordinates [3].

Results and Discussion

$PH_L \rightarrow P^+H_L^-$

The gas-phase energy change associated with the formation of the $P^+H_L^-$ radical-pair can be estimated by starting with experimentally measured redox potentials of P and H_L in the reaction center. The E_m for oxidation of P in *Rp. viridis* is $+0.50 \pm 0.02$ V with respect to the standard hydrogen electrode [57–59]. The E_m for reduction of H_L is less certain, with the four reported measurements ranging from -0.40 to -0.62 V [58–61]. As we shall discuss below, the value -0.62 V, which was measured by Shuvalov et al. [58] and supported subsequently by Rutherford et al. [60], appears to be the most consistent with the calculated electrostatic interactions of H_L with the surrounding protein. Using this value gives $\Delta G_\infty^w = 1.12$ eV or 25.8 kcal/mol. This free energy change describes the hypothetical formation of $P^+H_L^-$ when the two electron carriers are infinitely far apart. More precisely, it describes the reaction $2PH_L \rightarrow P^+H_L + PH_L^-$.

The change in electrostatic free energy associated with the formation of H_L^- in the X-ray structure was calculated to be -22.3 kcal/mol. Calculations of the electrostatic interactions of P and P^+ with their surroundings were carried out using two different treatments of the histidine residues that form the axial ligands of the BChls (histidines L173 and M200). In treatment 1, the imidazole rings of both histidines were considered to be part of the electron carrier; in treatment 2, they were considered to be part of the surrounding protein. The change in electrostatic energy associated with the formation of P^+ in the X-ray structure was calculated to be -18.2 kcal/mol in treatment 1,

TABLE I

Redox potentials, solvation energies and gas-phase energies [a]

Reaction[b]	Trim[c]	His[d]	E_m^D	E_m^A	ΔG_∞^w	ΔG_{sol}^{wD}	ΔG_{sol}^{wA}	$\sum \Delta G_{sol}^w$	α
$2\,PH_L \rightarrow P^+H_L + PH_L^-$			+0.50	−0.62	25.8				
	17	1				−21.2	−24.3	−45.5	71.3
		2				−36.8	−24.3	−61.1	86.9
	19	1				−21.7	−24.4	−46.1	71.9
		2				−37.3	−24.4	−61.7	87.5
+0.2 charge on Fe	19	1				−21.7	−24.9	−46.6	72.4
		2				−37.3	−24.9	−62.2	88.0
altered charges[e]	17	2				−34.5	−24.4	−59.0	84.8
$BPh^- + BChl \rightarrow BPh + BChl^-$			−0.50	−0.84	7.8				
	–	1				35.4	−33.8	1.6	6.2
	–	2				35.4	−23.7	11.7	−3.9

[a] Redox potentials are in *V*; energies and free energies, in kcal/mol. Superscript 'D' indicates the electron donor; 'A' indicates the acceptor. The solvation energies for $P \rightarrow P^+$ and $H_L \rightarrow H_L^-$ (ΔG_{sol}^{wD} and ΔG_{sol}^{wA}) include the reorganization energies ($\lambda_{P+} = 3.0$ kcal/mol and $\lambda_{H_L^-} = 2.0$ kcal/mol) in addition to the electrostatic energies (ΔG_{elec}).

[b] The electron donor and acceptor are evaluated independently at infinite separation. For the calculations on P, the *Rp. viridis* X-ray structure was trimmed in the same manner used for calculations on $P^+B_L^-$, i.e., to include all amino acid residues with one or more atoms within 17 Å (or where indicated, 19 Å) of either the center of P or the center of B_L. For the calculations on H_L, the structure included all residues within 17 (or 19) Å of either H_L or B_L. Except where specified otherwise, the Fe and all amino acid residues were assigned net charges of zero. The calculations for $BPh^- + BChl \rightarrow BPh + BChl^-$ refer to the free molecules in solution.

[c] Cutoff distance (Å) for including amino acid residues in the model (see text).

[d] Treatment of imidazole ligands of P, or the acetonitrile ligand of BChl in solution (see text).

[e] Partial charges on amino acid atoms assigned according to Weiner et al. [55], with adjustments for electrical neutrality. (The reorganization energies are still taken from calculations using the standard charge set, see Refs. 49 and 50.)

TABLE II

Calculated electrostatic energies and free energies [a]

Reaction	Trim[b]	His[c]	ΔV_{QQ}	$\Delta V_{Q\mu}$	ΔV_{ind}	ΔG_{bulk}	ΔG_{elec}	α	ΔG
$PH_L \rightarrow P^+ H_L^-$	17	1	−18.5	−9.9	−17.4	−0.1	−45.9	71.3	25.4
		2	−19.0	−21.2	−21.1	−0.2	−61.4	86.9	25.5
	19	1	−18.5	−9.1	−19.2	1.6	−45.1	71.9	26.8
		2	−19.0	−20.5	−22.8	1.6	−60.6	87.5	26.9
−0.2 chrge on Fe	19	1	−18.5	−10.4	−18.5	2.1	−45.2	72.4	27.2
		2	−19.0	−21.7	−22.1	2.1	−60.7	88.0	27.3
altered charges[d]	17	2	−19.0	−9.6	−29.4	−1.4	−59.3	84.8	25.5
all residues = Gly[e]	17	–	−19.0	2.3	–	−1.3	–	–	–
$PB_L \rightarrow P^+ B_L^-$	17	1	−29.9	−12.2	−9.7	0.9	−51.0	77.5	26.5
		2	−29.2	−15.3	−12.9	0.9	−56.5	83.0	26.5
	19	1	−29.9	−11.5	−10.6	1.2	−50.7	78.1	27.4
		2	−29.2	−14.6	−13.7	1.2	−56.2	83.6	27.4
+0.2 charge on Fe	19	1	(−29.9	−11.5	−10.6	1.2	−50.7)[f]	78.6	27.9
		2	(−29.2	−14.6	−13.7	1.2	−56.2)[f]	84.1	27.9
altered charges[d]	17	2	−29.2	−7.5	−18.3	0.1	−54.8	80.9	26.1
all residues = Gly[e]	17	–	−29.2	3.9	–	−0.4	–	–	–
Tyr-M208 = Phe[g]	17	1	−29.9	−7.1	−11.0	0.8	−47.1	77.5	30.4
		2	−29.2	−10.2	−14.2	0.8	−52.7	83.0	30.3
$P^+ B_L^- H_L \rightarrow P^+ B_L H_L^-$	17	1	−0.3	14.0	−7.5	−1.3	4.9	−6.2	−1.3
		2	−1.8	6.0	−8.0	−1.3	−5.2	3.9	−1.3
	19	1	−0.3	14.2	−8.3	−0.9	4.7	−6.2	−1.5
		2	−1.8	6.2	−8.8	−0.9	−5.3	3.9	−1.4
+0.2 charge on Fe	19	1	−0.3	13.0	−7.7	−0.5	4.6	−6.2	−1.6
		2	−1.8	5.0	−8.2	−0.5	−5.5	3.9	−1.6
altered charges[d]	17	2	−1.8	8.7	−10.0	−1.1	−4.2	3.9	−0.3
all residues = Gly[e]	17	–	−1.8	10.8	–	−1.4	–	–	–
Tyr-M208 = Phe[g]	17	1	−0.3	9.3	−6.3	−1.3	1.4	−6.2	−4.8
		2	−1.8	1.3	−6.6	−1.3	−8.5	3.9	−4.6
Glu-L104 COOH[h]	17	1	−0.3	15.7	−8.2	−1.3	5.9	−6.2	−0.3
		2	−1.8	7.7	−8.7	−1.3	4.1	3.9	−0.2
$P^+ B_L^- B_M \rightarrow P^+ B_L B_M^-$	17	1	−0.04	18.2	−9.5	−3.0	5.6	0.0	5.6
		2	0.02	18.4	−8.9	−3.0	6.5	0.0	6.5
	19	1	−0.04	15.8	−8.2	−2.9	4.6	0.0	4.6
		2	0.02	16.0	−7.6	−2.9	5.5	0.0	5.5
altered charges[d]	17	2	0.02	14.7	−6.6	−2.2	5.9	0.0	5.9
all residues = Gly[e]	17	–	0.02	3.1	—	−0.4	–	–	–
Tyr-M208 = Phe[g]	17	1	−0.04	13.4	−8.2	−3.0	2.2	0.0	2.2
		2	0.02	13.6	−7.5	−3.0	3.1	0.0	3.1
$P^+ H_L^- H_M \rightarrow P^+ H_L H_M^-$	17	–	0.08	2.3	1.1	−0.5	3.0	0.0	3.0
-Glu-L104 COOH[h]	17	–	0.08	0.4	2.1	−0.6	1.9	0.0	1.9

[a] Energies are in kcal/mol.
[b] Cutoff distance (Å) for including amino acid residues in the model (see text and Table I).
[c] Treatment of imidazole rings of axial histidines (see text).
[d] Partial charges on amino acid atoms assigned according to Weiner et al. [55], with adjustments for electrical neutrality.
[e] All amino acid residues replaced by glycine.
[f] The Fe is too far from B_L and P to be included in the models used for $P^+ B_L^-$; it contributes to α for the formation of this radical-pair because it is included in the calculation of ΔG_{sol}^{wA} for H_L^-.
[g] Tyrosine M208 replaced by phenylalanine.
[h] Partial charges removed from COOH atoms of Glu-L104. (These atoms were still considered to be polarizable.)

and −33.8 in treatment 2. This does not mean that the two treatments give different results for the total free energy change associated with the formation of P^+; the free energy change is simply divided differently between α and ΔG_{elec}. The calculated electrostatic energy change is more favorable in the second treatment, because it includes the interactions of the imidazole N atoms with the P^+ radical cation. As will be shown below, the results obtained with the two treatments converge when all of the contributions to ΔG are collected.

To obtain the complete solvation energies (ΔG^{w}_{sol}), the electrostatic energy changes for P^+ and H_L^- in the X-ray structure were combined with the reorganization energies (λ) obtained from the free energy perturbation treatment (see Fig. 2). The calculated reorganization energies were 2.0 kcal/mol for H_L^- and 3.0 kcal/mol for P^+. The larger reorganization energy for P^+ results primarily from movements of the axial histidine residues. If the partial charges on the imidazole rings were set to zero, the calculated reorganization energy for the formation of P^+ was 2.0 kcal/mol. Combining the reorganization energies and the electrostatic energy changes, ΔG^{w}_{sol} for the oxidation of P is calculated to be -21.2 kcal/mol in treatment 1 and -36.8 in treatment 2; ΔG^{w}_{sol} for the reduction of H_L is -24.3 kcal/mol. Subtracting the sums of the solvation energies ($\Sigma\Delta G^{w}_{sol}$) from ΔG^{w}_{∞} (Eqn. 8) gives a value of 71.3 kcal/mol for the gas-phase energy difference α in treatment 1 and 86.9 in treatment 2. The stabilizing effect of the imidazole ring thus results in a lower value of α in treatment 1. These calculations of α are sumamrized in Table I along with similar calculations in which the model was enlarged to include additional amino acid residues or different sets of atomic charges were used for the amino acids or the nonheme Fe atom.

The same two treatments of histidines L173 and M200 were used in calculations of the electrostatic free energy for the radical-pair $P^+H_L^-$ (ΔG_{elec} in Eqn. 2). The results are presented in Table II. Treatment 1 gave $\Delta G_{elec} = -45.9$ kcal/mol; treatment 2 gave -61.4. Adding these energies to the corresponding values of α (Eqn. 1) gives $\Delta G = 25.4$ kcal/mol for the reaction $PH_L \rightarrow P^+H_L^-$ in treatment 1 and 25.5 kcal/mol in treatment 2. The two treatments thus give essentially identical results for the overall change in free energy.

Table II lists the contributions that the individual terms of Eqn. 2 make to the overall ΔG_{elec} and ΔG for the formation of $P^+H_L^-$ from PH_L. The formation of the $P^+H_L^-$ radical-pair is favored, not only by the electrostatic interaction of P^+ with H_L^- (ΔV_{QQ}), but also by negative values of $\Delta V_{Q\mu}$ and ΔV_{ind}. This is the case in either of the two treatments of the axial histidine residues, although $\Delta V_{Q\mu}$ is substantially more negative when the imidazole rings are treated as part of the surroundings. The negative values of $\Delta V_{Q\mu}$ result primarily from favorable interactions with amino acid sidechains, and not from helix dipoles, because $\Delta V_{Q\mu}$ changes sign if all of the amino acid residues in the model are replaced by glycine (Table II). Induced dipoles in the protein and the surrounding membrane (ΔV_{ind}) are calculated to contribute -21.1 kcal/mol to ΔG_{elec} when the axial histidines are included in this part of the structure (treatment 2), and -17.4 kcal/mol when the imidazole rings are treated as parts of the electron carriers (treatment 1). If the polarizable atoms representing the membrane were omitted from the model, ΔV_{ind} was -20.4 kcal/mol in treatment 2 and -16.6 in treatment 1 (not shown in Table II). The membrane thus makes a relatively small contribution of about 0.8 kcal/mol to the electrostatic stabilization of the $P^+H_L^-$ radical-pair. Including the membrane in the model has little effect on the calculated free energy of $P^+H_L^-$, because the stabilization of P^+ and H_L^- also results in an increase in the calculated value α, which approximately balances the small negative contribution to ΔV_{elec}.

Essentially the same free energy was obtained for $P^+H_L^-$ when the calculations were performed with an alternative set of atomic charges for the amino acids (Tables I and II). Although $\Delta V_{Q\mu}$ depends strongly on the atomic charges, the self-consistent calculation of ΔV_{ind} makes the overall free energy relatively insensitive to the initial values of the charges.

The calculated free energy of $P^+H_L^-$ is about 1.4 kcal/mol higher if the cutoff distance for including amino acid residues in the model is increased from 17 to 19 Å (Table II). Enlarging the cutoff distance in this way increases the number of atoms in the model by about 26%, from 4419 to 5585 not including the polarizable atoms that were added to simulate the membrane. The effect on ΔG is due partly to a change of $+0.6$ kcal/mol in the calculated value of α (Table I), and to a change of about -0.8 kcal/mol in ΔG_{elec}. As will be discussed below, taking into account the charge on the nonheme Fe atom leads to a small additional increase in the calculated free energy of the radical-pair.

Using the results obtained with the larger model, and taking the effect of the Fe into account, the calculations put $P^+H_L^-$ approx. 27 kcal/mol above the ground state, or about 2.0 kcal/mol below the excited singlet state, P* (29.0 kcal/mol). These calculations refer to the unrelaxed $P^+H_L^-$ radical-pair in the static X-ray structure. The reorganization energy (λ) of $P^+H_L^-$ was calculated by the same perturbation treatment that was used for the individual radicals P^+ and H_L^-, and was found to be 5.0 kcal/mol. Thus, the free energy of the relaxed radical-pair is calculated to be approx. 22 kcal/mol. This is about 4 kcal/mol smaller than ΔG^{w}_{∞} (25.8 kcal/mol; Table I).

$PB_L \rightarrow P^+B_L^-$

Given the free energy of the $P^+H_L^-$ radical-pair, the free energy of $P^+B_L^-$ can be obtained by considering the reaction $P^+B_LH_L^- \rightarrow P^+B_L^-H_L$. It is necessary, however, to use the E_m values for BPh and BChl in polar organic solvents to estimate the gas-phase energy difference for electron transfer from $_L^-$ to B_L, because the E_m for the reduction of B_L cannot be measured directly in the reaction center. The E_m for the reduction of BPh *b* in dimethylformamide is -0.50 V [65]. The E_m for BChl *b* has not been measured accurately, but should be close to that for BChl *a* in butyronitrile, which is -0.84 V [63]. Subtracting the E_m values gives $\Delta G^{w}_{\infty} = 0.34$ eV or

7.8 kcal/mol. To calculate the solvation energies for the molecules in solution, we modeled the solvent with a grid of Langevin dipoles [48,49]. Again, parallel calculations were done in which the axial ligand of BChl was considered to be either part of the electron carrier (treatment 1) or part of the surroundings (treatment 2). The calculated change in solvation energy for the reduction of BChl to the radical anion ($BChl^-$) was −33.8 kcal/mol in treatment 1, and −23.7 in treatment 2; that for the reduction of BPh to BPh^- was −35.4 kcal/mol. Subtracting the change in the solvation energy for BPh from that for BChl gives $\Sigma\Delta G^{w}_{sol} = +1.6$ kcal/mol in treatment 1, and +11.7 kcal/mol in treatment 2. Subtracting the values of $\Sigma\Delta G^{w}_{sol}$ from $\Delta G^{w}_{(\infty)}$ gives $\alpha = +6.2$ kcal/mol for electron transfer from BPh^- to BChl in treatment 1, and −3.9 in treatment 2 (Table I).

Combining the gas-phase energy differences for electron transfer from P to H_L and from BPh^- to BChl gives $\alpha = 77.5$ kcal/mol for the reaction $PB_L \rightarrow P^+B_L^-$ in treatment 1 of the axial ligands, and 83.0 kcal/mol in treatment 2. Again, enlarging the model by using a cutoff distance of 19 instead of 17 Å changes these energies by about 0.6 kcal/mol.

Analogous treatments of the axial ligand of B_L (His L153) were used in calculations of the changes in electrostatic free energy (ΔG_{elec}) and total free energy for the reaction $PB_L \rightarrow P^+B_L^-$. Table II contains the results. Treatments 1 and 2 both put the unrelaxed $P^+B_L^-$ radical-pair approx. 1 kcal/mol above the unrelaxed $P^+H_L^-$, with the absolute value of the free energy again depending somewhat on the number of amino acid residues included in the model.

The individual terms that contribute to ΔG_{elec} and ΔG for the formation of $P^+B_L^-$ are given in Table II. The formation of $P^+B_L^-$, like that of $P^+H_L^-$, is favored by negative values of $\Delta V_{Q\mu}$ and ΔV_{ind}. Again, the negative $\Delta V_{Q\mu}$ results mainly from interactions with amino acid side-chains, because $\Delta V_{Q\mu}$ becomes positive if all of the amino acid residues in the model are replaced by glycine. Apart from the histidine residues, the largest individual contribution to $\Delta V_{Q\mu}$ comes from Tyr-M208 and reflects interactions with the phenolic -OH group. If Tyr-M208 is replaced by phenylalanine, the calculated $\Delta V_{Q\mu}$ becomes less favorable by approx. 5 kcal/mol (Table II). An increase in the magnitude of the induced-dipole energy (ΔV_{ind}) compensates for part of the decrease in $\Delta V_{Q\mu}$, so that the overall change in ΔG_{elec} is approx. 3.9 kcal/mol. As with $P^+H_L^-$, the calculated free energy of $P^+B_L^-$ is not very sensitive to the choices of the atomic charges for the amino acids.

$P^+B_L^-H_L \rightarrow P^+B_LH_L^-$

Also shown in Table II are the components of ΔG_{elec} and ΔG for electron transfer from B_L^- to H_L in the presence of P^+. This reaction is calculated to be downhill by approx. 1.4 kcal/mol with either treatment of the axial ligand of B_L. This agrees reasonably well with the result obtained by subtracting the calculated free energies of the two charge-separation reactions, $P\,B_L \rightarrow P^+B_L^-$ and $P\,H_L \rightarrow P^+H_L^-$. The reaction involves an unfavorable change in $V_{Q\mu}$, which again, is due partly to the stabilization of B_L^- by Tyr-M208. If the tyrosine is replaced by phenylalanine, the overall ΔG for electron transfer from B_L^- to H_L becomes more negative by 3.4 kcal/mol. Glutamic acid L104, which probably forms a hydrogen bond to the ketone group on ring V of H_L [2,15], has a small effect in the opposite direction. If the partial charges on the carboxylic acid group of this residue are omitted, the free energy difference between $P^+B_L^-$ and $P^+H_L^-$ decreases by about 1 kcal/mol. The polypeptide backbone also appears to be oriented so as to stabilize $P^+B_L^-$ relative to $P^+H_L^-$, because replacing all of the side-chains by glycine leaves a large, positive $\Delta V_{Q\mu}$ (Table II). As will be discussed below, including the charges on the nonheme Fe and on the ionizable amino acid residues within 19 Å of B_L or H_L increases the calculated ΔG for electron transfer from B_L^- to H_L to approx. 2.0 kcal/mol.

$PB_M \rightarrow P^+B_M^-$

The free energy of the $P^+B_M^-$ radical-pair can be obtained by considering the charge-transfer reaction $P^+B_L^-B_M \rightarrow P^+B_LB_M^-$. It seems an acceptable approximation to neglect possible effects of the small structural differences between B_L and B_M, and to take the gas-phase energy difference to be zero for electron transfer from one of these BChls to the other, so that $\Delta G = \Delta G_{elec}$. Again, we calculated ΔG_{elec} with two different treatments of the axial ligands of the BChls (His L153 and His M180). Although treatment 2 gave somewhat larger values than treatment 1, both treatments put $P^+B_M^-$ about 6 kcal/mol above $P^+B_L^-$ (Table II).

The individual contributions to ΔG_{elec} and ΔG for electron transfer from B_L^- to B_M are included in Table II. The increase in G_{elec} associated with this reaction results from a large, positive value of $\Delta V_{Q\mu}$, which is only partially compensated for by negative values of ΔV_{ind} and ΔG_{bulk}. Again, the stability of $P^+B_L^-B_M$ relative to $P^+B_LB_M^-$ appears to be due largely to favorable interactions of B_L^- with the -OH group of Tyr M208. If the tyrosine is replaced by phenylalanine, the calculated free energy difference between $P^+B_L^-$ and $P^+B_M^-$ decreases by about 50%.

The conclusion that $P^+B_M^-$ is about 6 kcal/mol higher in free energy than $P^+B_L^-$ disagrees with a report by Treutlein et al. [69], who calculated mean electrostatic potentials at the positions of the electron carriers. In their calculation, adding electron to B_M was found to be more favorable than adding an electron to B_L, by about 15 kcal/mol. Treutlein et al. [69] apparently took all ionizable amino acid residues to be in the charged

forms and did not consider the solvation of these ions by the surrounding medium and by induced dipoles in the protein. As is discussed below, most of the potentially ionizable amino acids near B_L and B_M seem unlikely to be charged, and the charged residues in the more distant, polar regions of the protein probably are well solvated. Results that agree qualitatively with ours were obtained by Yeates et al. [56], who also took all ionizable residues to be charged, but who scaled the electrostatic interactions by using bulk dielectric constants for the protein, membrane and solvent.

$PH_M \rightarrow P^+H_M^-$

The free energy of the $P^+H_M^-$ radical-pair can be obtained by considering the charge-transfer reaction $P^+H_L^- \rightarrow P^+H_M^-$. As for the reaction between B_L^- and B_M, we take α for electron transfer from H_L^- to H_M to be zero. ΔG_{elec} was calculated to be 3.0 kcal/mol, which is significantly smaller than the values of about 6 kcal/mol obtained for electron transfer from B_L^- to B_M.

Table II shows the components of ΔG_{elec} and ΔG for electron transfer from H_L^- to H_M. $\Delta V_{Q\mu}$, ΔV_{ind} and ΔG_{bulk} are all considerably smaller than the corresponding terms for the reaction from B_L^- to B_M. The positive value of $\Delta V_{Q\mu}$ is due partly to the loss of the favorable interactions of H_L^- with the carboxylic acid group of Glu acid L104. If the partial charges on the carboxylic acid group are omitted, the overall values of ΔG_{elec} and ΔG decrease by about 1 kcal/mol.

Effects of charges on the Fe and ionizable amino acid residues

Because the nonheme Fe atom is located more than 17 Å from any of the BChl and BPh molecules, it was not included in the models that were trimmed with this cutoff distance. It was, however, present in some of the larger models obtained with a cutoff radius of 19 Å. Calculations on these models were carried out both with and without a charge of +0.2 on the Fe. The choice of a small effective charge was designed to reflect the fact that the Fe is well solvated by the negatively charged carboxylate group of glutamic acid M232 and other polar groups, some of which lie outside of the model. It has been argued previously [48] that the effective dielectric constants for ionized groups in proteins are relatively large. Adding a charge of +0.2 to the Fe makes ΔG_{sol}^{wA} for the reduction of H_L more negative by 0.6 kcal/mol, and thus increases the calculated value of α for the formation of $P^+H_L^-$ or $P^+B_L^-$ (Table I). The calculated free energy of $P^+B_L^-$ increases by the same amount, and that of $P^+H_L^-$ by 0.5 kcal/mol (Table II). The calculated effect of the Fe is thus to increase the free energy difference between $P^+B_L^-$ and $P^+H_L^-$ by about 0.1 kcal/mol. A somewhat larger effect is obtained in the direct calculation on the reaction $P^+B_L^-H_L \rightarrow P^+B_LH_L^-$. In this calculation, a charge of +0.2 on the Fe increases the free energy difference between $P^+B_L^-$ and $P^+H_L^-$ by about 0.3 kcal/mol (Table II). Some calculations also were carried out with the full formal charge of +2.0 on the Fe and a charge of −1.0 on glutamic acid M232. Using these charges gave a value of −2.6 kcal/mol for the free energy change accompanying electron transfer from B_L^- to H_L (data not shown in Table II). This is 1.2 kcal/mol larger than the value obtained when the Fe was uncharged. However, the Fe is probably too close to the edge of the microscopic model for this calculation to be reliable. The PDLD method is likely to underestimate the compensating dielectric effects associated with charge–charge interactions in proteins when the charged species are this far apart, particularly when one or both of the charged species have relatively small ionic radii [48]. The calculations are subject to larger errors than calculations on the interactions between larger radicals such as P^+, B_L^- and H_L^-, where the charges are spread over many atoms.

The charge on the Fe would not be expected to influence the energy difference between $P^+B_L^-$ and P^+B_M, or between $P^+H_L^-$ and $P^+H_M^-$, because the Fe is located close to the rotational symmetry axis.

In most of the calculations described above, the ionizable amino acid residues were assumed to be in their neutral forms. (Glutamate M232 was given a net negative charge only in some of the calculations on the Fe.) Again, this is in accord with the view that any of these residues that are, in fact, charged will be screened by relatively large dielectric constants [48]. Excluding the histidines that serve as axial ligands of the BChls, there are five residues that have potentially charged side chains within 20 Å of B_L in the *Rp. viridis* reaction center: Asp-L60, Asp-L155, Arg-L135, Arg-C15 and His-L168. Excluding Glu-L104 and the ligands of P and the Fe, there are an additional five residues with ionizable groups within 20 Å of the center of H_L: Asp-H36, Arg-L103, Arg-H33, Glu-L106, and His-L116. The ionizable groups of Arg-H33 and Asp-H36 are located close together and probably form an ion pair. Such a pair would have little effect on the energetics of the electron-transfer reactions because its positively and negatively charged groups are nearly equidistant from H_L. To examine which of the other eight residues are likely to be charged at physiological pH, we calculated the electrostatic solvation energies for their side-chains in the protein and for the free amino acids in water. The ionizations of Asp-L60, Arg-C15, Arg-L103 and Glu-L106 all were found to be at least as favorable as those of the same amino acids in water, indicating that these four residues probably are charged throughout the pH range of 7 to 9 over which the reaction center operates well. The ionizations of Arg-L135 and Asp-L155 were both found to be about 11 kcal/mol less favorable than the corresponding ionizations in solution, indicating

that these two residues are unlikely to be charged. Protonation of His-L116 was calculated to be 3 kcal/mol less favorable than protonation of histidine in solution, and that of His-L168 was found to be 5 kcal/mol less favorable. The calculated solvation energies would put the pK_a value of His-L116 in the range of 4, and that of His-L168 below 3. (Histidine L168 forms a hydrogen bond to the acetyl group of BChl P_L, and thus is in a position where its protonation might be expected to perturb the absorption spectrum of the reaction center; there is no evidence that this happens above pH 5.) It therefore appears that, neglecting Arg-H33 and Asp-H36, Asp-L60, Arg-C15, Arg-L103 and Glu-L106 are the only residues within 20 Å of B_L or H_L that are likely to be charged under physiological conditions. This is in accord with the hydrophobic nature of most of the amino acids in the central part of the reaction center.

The charged groups of Asp-L60, Arg-C15, Arg-L103 and Glu-L106 are all relatively far from the electron carriers, making it difficult to evaluate their effects on the radical-pair states reliably. Measuring from the center of B_L, the distance to the C_γ carbon of Asp-L60 is about 17.3 Å, and the distance to C_ζ of Arg-C15 is about 19.9 Å (Fig. 1). From the center of H_L, the distance to C_ζ of Arg-L103 is about 14.1 Å and that to C_δ of Glu-L106 is about 19.5 Å. As we noted above in connection with the Fe, the PDLD treatment probably underestimates the dielectric effects of the protein for small, widely-separated ions. However, a rough estimate of the contribution of these groups to the free energy difference between $P^+B_L^-$ and $P^+H_L^-$ can be obtained as follows. The combined effect of charging Asp-L60, Arg-C15, Arg-L103 and Glu-L106 is to reduce $\Delta V_{Q\mu}$ for the reaction $P^+B_L^-H_L \rightarrow P^+B_LH_L^-$ by 5.0 kcal/mol. If we assume that this interaction is screened by an average effective dielectric constant of 10, adding the charges to these residues would contribute about -0.5 kcal/mol to ΔG for electron transfer from B_L^- to H_L. This would change the calculated value of δG for this reaction from -1.4 kcal/mol to -1.9 kcal/mol, or to about -2.1 kcal/mol if a charge of $+0.2$ is used on the Fe.

Possible contributions of charged residues to the free energy difference between $P^+B_L^-$ and $P^+B_M^-$ also were considered. The residues with potentially charged side chains within 20 Å of either B_L or B_M include Asp-L60, Asp-L155, Arg-L135, Arg-C15 and His-L168, which were discussed above, and also Asp-M182, Glu-M76, Glu-M171 and His-M162. The ionizations of these last four residues all were calculated to be substantially less favorable than those of the amino acids in solution. The only marginal case is Glu-M76, for which the calculated pK_a is about 9.6. Thus the only charged residues that are close enough to either B_L or B_M to contribute significantly to the energy difference between $P^+B_L^-$ and $P^+B_M^-$ are probably Asp-L60 and Arg-C15. The combined effect of ionizing these two residues is to reduce $\Delta V_{Q\mu}$ for the reaction $P^+B_L^- \rightarrow P^+B_M^-$ by 1.2 kcal/mol. If we again assume that this effect would be screened by an effective dielectric constant of 10, including the charges changes the ΔG for this reaction by only 0.1 kcal/mol. Including Glu-M76 would give a small effect in the opposite direction.

The parts of the reaction center that protrude from the membrane contain a number of additional residues that are likely to be charged, particularly in the cytochrome and H subunits. Because the charged groups of these residues are all more than 20 Å from the electron carriers, and are likely to be well solvated by water and the surrounding protein, their net effects on the energies of the radical-pairs probably are negligible. (For a discussion of related cases, see Refs. 48, 52).

The charge distribution in P^+

In the preceding calculations, the positive charge of P^+ was assumed to be distributed equally between BChls, P_L and P_M. EPR, ENDOR and TRIPLE resonance measurements are consistent with an equal distribution of the charge in *Rb. sphaeroides* reaction centers, but suggest that in *Rp. viridis* about 70% of the positive charge may be concentrated on one of the two BChls [70–74]. The experimental results do not indicate unambiguously which molecule has the larger charge, however, and it may be possible to explain the data in other ways [70–71]. Calculations of the electrostatic energies therefore were carried out with a range of charge distributions. As shown in Table III, the electrostatic interactions of P^+ with its surroundings are improved by concentrating the positive charge on P_M. Essentially the same trend is seen whether the axial histidine ligands are considered to be part of P or part of the surroundings, which means that it is due predominantly to the interactions of the BChls with residues other than the histidines. No individual residue stands out in this regard. Judging from their contributions to $\Delta V_{Q\mu}$, Ser-L176, Val-L177, Thr-L248, Leu-M184, Cys-M197 and His-M200 all favor localization of a positive charge on P_M; Val-L157, Trp-L167, His-L168, His-L173, Ser-M188 and Ile-M204 favor placing the charge on P_L. Similar results were obtained when the X-ray structure was trimmed in two different ways (structures 'A' and 'B' in Table III), or when Arg-L135 was given a positive charge (not shown in Table III). (Although we concluded above that Arg-L135 is unlikely to be charged at physiological pH, its potential contribution to the charge distribution in P was investigated because the ionizable group is considerably closer to P_L than to P_M.) The same dependence of ΔG_{elec} on the charge distribution also was obtained when the alternative set of atomic charges was used for the amino acids, although the relative contributions of ΔV_{Qm} and ΔV_{ind} to ΔG_{elec} again depended on the values used for the charges (Table III).

TABLE III

Electrostatic effects [a] *of the protein on the charge distribution in* P^+

Reaction[b]	His[c]	P_L^+/P_M^+[d]	$\Delta V_{Q\mu}$	ΔV_{ind}	ΔG_{bulk}	ΔG_{elec}
$P \rightarrow P^+$ in structure A	1	0.0/1.0	−1.3	−15.8	−5.4	−22.5
		0.1/0.9	−0.8	−14.7	−5.3	−20.9
		0.3/0.7	0.2	−13.4	−5.2	−18.4
		0.5/0.5	1.1	−13.0	−5.1	−16.9
		0.7/0.3	2.1	−13.5	−5.0	−16.4
		0.9/0.1	3.1	−14.8	−5.0	−16.7
		1.0/0.0	3.6	−15.9	−5.0	−17.2
	2	0.0/1.0	−13.5	−20.9	−5.4	−39.7
		0.1/0.9	−12.9	−19.5	−5.3	−37.8
		0.3/0.7	−11.9	−17.6	−5.2	−34.7
		0.5/0.5	−10.8	−16.7	−5.1	−32.7
		0.7/0.3	−9.8	−16.9	−5.0	−31.7
		0.9/0.1	−8.7	−18.1	−5.0	−31.8
		1.0/0.0	−8.2	−19.2	−5.0	−32.3
altered charges[e]	2	0.0/1.0	−3.0	−28.3	−5.4	−36.7
		0.1/0.9	−2.8	−26.8	−5.3	−34.9
		0.3/0.7	−2.6	−24.5	−5.2	−32.3
		0.5/0.5	−2.3	−23.3	−5.1	−30.7
		0.7/0.3	−2.0	−23.1	−5.0	−30.2
		0.9/0.1	−1.8	−24.0	−5.0	−30.7
		1.0/0.0	−1.6	−24.8	−5.0	−31.4
$P \rightarrow P^+$ in structure B	1	0.5/0.5	−1.7	−11.4	−5.1	−18.2
	2	0.0/1.0	−15.5	−19.6	−5.3	−40.4
		0.1/0.9	−15.1	−18.2	−5.3	−38.5
		0.3/0.7	−14.2	−16.3	−5.2	−35.6
		0.5/0.5	−13.4	−15.4	−5.1	−33.8
		0.7/0.3	−12.5	−15.6	−5.0	−33.1
		0.9/0.1	−11.7	−16.8	−4.9	−33.4
		1.0/0.0	−11.3	−17.8	−4.9	−33.9
$P \rightarrow P^+$ in structure C	2	0.1/0.9	−18.7	–	–	–
		0.5/0.5	−18.2	–	–	–
		0.9/0.1	−17.7	–	–	–
$P \rightarrow P^+$ in structure D	2	0.1/0.9	−19.8	–	–	–
		0.5/0.5	−20.4	–	–	–
		0.9/0.1	−21.1	–	–	–

[a] Energies are in kcal/mol. Interactions between P_L and P_M are not included (P^+ is treated as an entity with an assumed charge distribution). The states considered here are adiabatic states, not basis states.

[b] Structure A included all of the pigments and the 181 amino acid residues that have one or more atoms within 17 Å of either the center of P_L or the center of P_M. Structure B was that used for calculations on $P^+ B_L^-$; it included all the pigments and the 183 amino acid residues that have one or more atoms within 17 Å of either the center of P or the center of B_L. Structure C included only P_L, P_M, their phytol side-chains, histidines L168, L173 and M200, Thr-L248 and Tyr-M195. Structure D included Val-L157, Tyr-M208, and Ala-M278 in addition to the components of Structure C.

[c] Treatment of imidazole rings of axial histidines (see text).

[d] Net positive charges on P_L and P_M.

[e] Partial charges of amino acid atoms assigned according to Weiner et al. [55], with adjustments for electrical neutrality.

Plato et al. [71–75] have described molecular orbital calculations that suggested that electrostatic interactions with nearby amino acid residues favor a localization of the charge of P^+ on P_L. Michel-Beyerle et al. [16] also discussed the electrostatic interactions of P^+ with neighboring amino acids; they found little preference for the positive charge to concentrate on either P_L or P_M. The major reasons for these apparent disagreements with our results are probably that Plato et al. and Michel-Beyerle et al. considered only eight amino acid residues in the immediate vicinity of P and did not include the effects of induced dipoles. Restricting the model to a small number of amino acids of course makes the results sensitive to exactly which residues one includes. When we reduced the model to the five residues that form covalent bonds or hydrogen bonds to the BChls, and omitted induced dipoles, we still obtained a small preference for the charge to concentrate

TABLE IV

Sensitivity of calculated energies to the assumed charge distribution in P^+ [a]

Reaction	P_L^+/P_M^+ [b]	ΔV_{QQ}	$\Delta V_{Q\mu}$	ΔV_{ind}	ΔG_{bulk}	ΔG_{elec}	α	ΔG
$PH_L \rightarrow P^+ H_L^-$	0.1/0.9	−18.2	−22.7	−24.3	−0.5	−65.7	91.6	25.9
	0.5/0.5	−19.0	−21.2	−2.11	−0.2	−61.4	86.9	25.5
	0.9/0.1	−19.7	−19.7	−21.9	0.2	−61.2	86.5	25.3
$PB_L \rightarrow P^+ B_L^-$	0.0/1.0	−29.2	−16.3	−16.2	0.5	−61.2	89.6	28.4
	0.1/0.9	−29.2	−16.1	−15.1	0.6	−59.8	87.7	27.9
	0.3/0.7	−29.2	−15.7	−13.5	0.7	−57.6	84.8	27.2
	0.5/0.5	−29.2	−15.3	−12.9	0.9	−56.6	83.0	26.5
	0.7/0.3	−29.2	−15.0	−13.2	1.0	−56.3	82.3	26.0
	0.9/0.1	−29.2	−14.6	−14.4	1.1	−57.1	82.6	25.5
	1.0/0.0	−29.1	−14.4	−15.4	1.1	−57.8	83.1	25.3
$P^+ B_L^- H_L \rightarrow P^+ B_L H_L^-$	0.1/0.9	−1.8	6.0	−8.2	−1.3	−5.3	3.9	−1.4
	0.5/0.5	−1.8	6.0	−8.0	−1.3	−5.2	3.9	−1.3
	0.9/0.1	−1.8	5.9	−7.8	−1.4	−5.1	3.9	1.2
$P^+ B_L^- B_M \rightarrow P^+ B_L B_M^-$	0.1/0.9	0.02	20.4	−10.5	−3.2	6.7	0.0	6.7
	0.5/0.5	0.02	18.4	−8.9	−3.0	6.4	0.0	6.5
	0.9/0.1	0.02	16.4	−7.3	−2.8	6.3	0.0	6.3

[a] Energies are in kcal/mol. Interactions between BChls P_L and P_M are not considered. The cutoff distance for including amino acid residues in the structure was 17 Å. Axial imidazole rings were treated as part of the surroundings (treatment 2). The values of α for $P^+ H_L^-$ and $P^+ B_L^-$ are based on the evaluation of ΔG_{sol}^{w} for P^+ in structure B (Table III). The states considered here are adiabatic states of the system, not basis states.

[b] Net positive charges on P_L and P_M.

on P_M (Table III, 'structure C'). Adding three residues to structure C (and still neglecting ΔV_{ind}) resulted in a small preference for the positive charge to concentrate on P_L (Table III, 'structure D'). This last structure is the one considered by Plato et al. [74] and Michel-Beyerle et al. [16], and our results on it agree with theirs. However, the results obtained by using a larger model and including induced dipoles seem likely to be more meaningful.

Table IV shows how varying the assumed charge distribution in P^+ affects the calculated energies of other states of the system. The final free energies are not very sensitive to the charge distribution. Placing 90% of the charge on P_M improves the electrostatic stabilization of $P^+ B_L^-$ by 3.3 kcal/mol (changing ΔG_{elec} from −56.5 to −59.8 kcal/mol) but results in a small increase (1.4 kcal/mol) in the calculated free energy of $P^+ B_L^-$ because an increase in α outweighs the change in ΔG_{elec}. The change in ΔG is somewhat smaller (-1.0 kcal/mol) if 90% of the charge is put on P_L. There are only very small effects on the calculated free energy difference between $P^+ B_L^-$ and $P^+ B_M^-$, on the difference between $P^+ B_L^-$ and $P^+ H_L^-$, or on the free energy of $P^+ H_L^-$. In the case of $P^+ H_L^-$, changes in ΔG_{elec} are nearly balanced by opposite changes in α.

Although the calculations shown in Table III indicate that interactions of P^+ with the protein favor a concentration of the positive charge on P_M, they do not allow one to predict the actual charge distribution because they do not include the interactions of P_L and P_M with each other. The two BChls are simply treated as an entity with a known E_m and an assumed charge distribution. To predict the actual charge distribution on the basis of the crystal structure, it is necessary to consider the energies of the pure $|P_L^+\rangle$ and $|P_M^+\rangle$ basis states, in which the full charge is on either P_L or P_M alone, and to evaluate the resonance interactions that mix these two states to give the adiabatic eigenstate, P^+. The resonance interactions act to disperse the positive charge over the two molecules.

The difference between the energies of $|P_L^+\rangle$ and $|P_M^+\rangle$ depends on two factors, one of which is the difference between the intrinsic orbital energies of BChls, P_L and P_M. Plato et al. [71–75] and Barkigia et al. [76] have noted that the macrocyclic ring system of P_M is less planar than that of P_L, and both groups concluded that this would tend to favor the oxidation of P_L relative to P_M. Barkigia et al. [76] calculated that the highest occupied molecular orbital of P_L is about 0.03 eV (0.7 kcal/mol) higher in energy than that of p_M. However, gas-phase quantum mechanical calculations typically tend to overestimate such effects, which usually are compensated when the environment is included. A more important factor, probably, is the difference between the electrostatic interactions of P_L^+ and P_M^+ with their surroundings.

Calculations of the electrostic energies of the $|P_L^+\rangle$ and $|P_M^+\rangle$ basis states are summarized in Table V. For the calculations on $|P_L^+\rangle$, P_M was considered to be part of the surroundings and its interactions with P_L or P_L^+ were included in $\Delta V_{Q\mu}$ and ΔV_{ind}; for the calculations on $|P_M^+\rangle$, P_L was considered to be part of the surround-

TABLE V

Electrostatic energies of basis states [a]

Reaction	Structure [b]	His [c]	ΔV_{QQ}	$\Delta V_{Q\mu}$	ΔV_{ind}	ΔG_{bulk}	ΔG_{elec}
$P_M \rightarrow P_M^+$	[d]	–	–	0.33	−4.1	–	−3.8
$P_L \rightarrow P_L^+$		–	–	−0.28	−5.2	–	−5.5
$P_M \rightarrow P_M^+$	A	1	–	−3.3	−17.2	−5.4	−25.9
$P_L \rightarrow P_L^+$			–	1.7	−19.6	−5.0	−22.9
$P_M \rightarrow P_M^+$	B	1	–	−4.9	−16.3	−5.4	−26.6
$P_L \rightarrow P_L^+$			–	−1.6	−18.1	−4.9	−24.5
$P_M \rightarrow P_M^+$	A	2	–	−13.3	−21.8	−5.4	−40.5
$P_L \rightarrow P_L^+$			–	−8.4	−21.8	−5.0	−35.2
$P_M \rightarrow P_M^+$	B	2	–	−14.7	−21.0	−5.4	−41.1
$P_L \rightarrow P_L^+$			–	−11.7	−20.3	−4.9	−36.9
$P_M B_L \rightarrow P_M^+ B_L^-$	B	1	−30.2	−14.4	−13.0	0.5	−57.0
$P_L B_L \rightarrow P_L^+ B_L^-$			−29.2	−14.1	−17.5	1.0	−59.6
$P_M B_L \rightarrow P_M^+ B_L^-$	B	2	−28.1	−17.1	−17.3	0.5	−61.9
$P_L B_L \rightarrow P_L^+ B_L^-$			−29.6	−14.2	−18.7	1.1	−61.4
$P_M H_L \rightarrow P_M^+ H_L^-$	E	1	−17.8	−13.3	−22.4	−0.6	−54.2
$P_L H_L \rightarrow P_L^+ H_L^-$			−19.0	−10.6	−23.6	0.3	−52.9
$P_M H_L \rightarrow P_M^+ H_L^-$	E	2	−17.7	−23.5	−26.9	−0.6	−68.6
$P_L H_L \rightarrow P_L^+ H_L^-$			−19.6	−20.7	−25.7	0.2	−65.1

[a] Energies are in kcal/mol. Electrostatic interactions with the other BChl of P are included in $\Delta V_{Q\mu}$ and ΔV_{ind}. The calculations do not include the reorganization energies and they neglect intrinsic orbital energy differences between P_L and P_M.

[b] Structures A and B were as in Table III; E included all amino acids within 17 Å of the center of P or H_L.

[c] Treatment of imidazole rings of axial histidines (see text).

[d] No amino acid residues and no pigments other than P_L and P_M.

ings. The first two lines in the table show the results of considering only the electrostatic interactions of the two BChls with each other. These interactions are more favorable for P_L^+ than they are for P_M^+, by about 1.7 kcal/mol. This agrees with the molecular orbital calculations of Plato et al. [71–75], which indicated that, in the 'bare' $P_L P_M$ dimer, the positive charge of the radical cation would tend to concentrate on P_L.

When the dimer is surrounded by the protein, the more favorable interactions of P_M^+ with the surrounding amino acid residues appear to predominate over the electrostatic interactions between P_L and P_M. The overall electrostatic stabilization of $|P_M^+\rangle$ is larger than that of $|P_L^+\rangle$ by 2 to 5 kcal/mol, depending on the treatment of the axial histidines and on the boundaries of the structure that is considered (Table V).

The off-diagonal interaction matrix element that mixes the $|P_L^+\rangle$ and $|P_M^+\rangle$ basis states, U_{LM}, was calculated by methods that have been described previously [47,66–68], and was found to be -910 cm^{-1} (-2.59 kcal/mol). If we use for the basis-state energies the values of ΔV_{elec} obtained with treatment 1 of the histidines and structure A (-25.9 and -22.9 kcal/mol), diagonalizing the 2×2 Hamiltonian matrix gives -27.4 kcal/mol for the energy of the lower eigenstate. This state has the composition $0.87|P_M^+\rangle + 0.50|P_L^+\rangle$. The upper eigenstate, which has the composition $0.50|P_M^+\rangle - 0.87|P_L^+\rangle$ lies about 6 kcal/mol above the lower state. Taking the squares of the coefficients, one finds that the ratio of the charges on the two BChls in the lower eigenstate would be 0.75/0.25 in favor of P_M^+, which appears to be consistent with the ENDOR, EPR and TRIPLE resonance data [70–73]. The energies obtained with structure B give -28.3 kcal/mol for the lower eigenvalue and 0.68/0.32 for the charge ratio, which also is consistent with the experimental data. With treatment 2 of the histidines, the corresponding charge ratios are 0.86/0.14 in structure A and 0.82/0.18 in structure B, which are somewhat more asymmetric than the magnetic resonance data suggest. Lowering the energy of the $|P_L^+\rangle$ basis state by 0.7 kcal/mol, as suggested by the molecular orbital calculations [76], would make the calculated distributions of charge in the eigenstates more symmetrical.

The electrostatic energies in Table V do not include the reorganization energy, λ, which applies to the adiabatic eigenstates rather than to the basis states. Because the protein relaxes in response to the average charge distribution in the lower adiabatic state, the reorganization would be expected to stabilize this eigenstate more than it does the upper state, increasing the asymmetry of the charge distribution.

Higher-energy eigenstates of $P^+H_L^-$ and $P^+B_L^-$

The $P^+H_L^-$ radical-pair also can be described as an adiabatic state that diagonalizes a matrix of basis configurations, each of which involves only one of the two possible electron donors, P_L or P_M. Estimates of the electrostatic free energies of the basis configurations $|P_L^+H_L^-\rangle$ and $|P_M^+H_L^-\rangle$ are included in Table V. Again, the state involving P_M^+ is calculated to have the lower energy. The $|P_L^+H_L^-\rangle$ and $|P_M^+H_L^-\rangle$ basis configurations are mixed by the same off-diagonal matrix element U_{LM} that mixes $|P_L^+\rangle$ and $|P_M^+\rangle$ (-2.59 kcal/mol). Diagonalizing the 2×2 matrix gives a pair of eigenstates that are separated by 5.3 kcal/mol with treatment 1 of the axial histidines, or by 6.3 kcal/mol with treatment 2. Thus the higher-energy eigenstate of the unrelaxed $P^+H_L^-$ radical-pair probably lies about 6 kcal/mol above the species considered in Table II. Again, the difference between the two eigenvalues would be somewhat smaller if a correction were applied for the molecular orbital energy difference between $|P_M^+\rangle$ and $|P_L^+\rangle$.

The same considerations apply to $P^+B_L^-$. The electrostatic free energies of the $|P_L^+B_L^-\rangle$ and $|P_M^+B_L^-\rangle$ basis configruations are given in Table V. In this case, the two treatments of the histidine ligands give somewhat different results. $|P_L^+B_L^-\rangle$ is slightly below $|P_M^+B_L^-\rangle$ in treatment 1, but above it in treatment 2. Diagonalizing the interaction matrix puts the upper eigenstate between 5 and 6 kcal/mol above the lower, depending on the treatment of the histidines.

Error analysis

In any calculation of electrostatic free energies in proteins, one faces the difficult problem of evaluating the reliability of the results. Two general types of errors can be important: errors in convergence and errors in accuracy. Convergence errors in the present case are those associated with calculating the self-consistent interactions of the induced dipoles or of the Langevin dipoles in the calculations on BChl and BPh in solution. We evaluated these errors by examining the results after each iteration of the algorithm, and by repeating the calculations with different grids for the Langevin dipoles. ΔV_{ind} always converged quickly and monotonically and could be extrapolated accurately to an asymptote after five or six iterations. (We used a nonlinear-least-squares fitting procedure to do this systematically.) The Langevin energies for BChl and BPh converged more slowly, undergoing damped oscillations, and approx. 50 iterations were needed in order to reduce the uncertainty in the asymptote to a few tenths of a kcal/mol. There is a residual uncertainty of approx. ± 0.5 kcal/mol in the convergence of the langevin calculations, relating mainly to the choices of the origins of the grids; this uncertainty was reduced by using a sufficiently fine grid spacing and by averaging the results obtained with five different grids. The grids used to model induced dipoles in the membrane surrounding the reaction center are less critical because most of the atoms placed on these grids are relatively far from the electron carriers.

Errors in the accuracy or physical significance of the calculations could arise from neglecting or oversimplifying any of the key contributions to ΔV_{elec}, such as the effects of induced dipoles in the protein or the surrounding solvent. This point was discussed above in connection with P^+. Including all of the important contributions to ΔG_{elec}, and treating them in a detailed and self-consistent manner, still leaves the possibility of errors due to (a) uncertainties in the E_m values used in the calculations of α, (b) considering too restricted a region of the protein or the solvent, (c) an inappropriate treatment of groups that are bonded covalently to the electron carriers, (d) neglecting significant structural differences between BChl or BPh in solution and in the reaction center, (e) poor choices of the residual charges or polarizabilities of the atoms, or (f) errors in the X-ray structure. We shall comment briefly on each of these sources of error.

(a) The calculated free energies of the radical-pairs depend linearly on the E_m values assigned to the individual electron carriers. The most problematical E_m is that of H_L because of the disagreement among the experimental values that have been reported [58–61]. It is possible that some of the experimental measurements were compromised by a failure of H_L to equilibrate rapidly with the external electrodes that were used to measure the redox potential.

Electrostatic stabilization of H_L^- in the reaction center appears to be significantly weaker than that of BPh^- in solution (-24.3 to -26.3 kcal/mol compared to -35.4 kcal/mol, Table I). This implies that the effective E_m of H_L should be more negative than the E_m of BPh b in vitro, which is -0.50 V [65]. The E_m value of -0.62 V measured by Shuvalov et al. [58] agrees with this expectation, and therefore seems preferable to the less negative value of -0.40 V reported by Prince et al. [59]. Shopes and Wraight [61] obtained an intermediate value of -0.52 V, which also would be consistent with our results. Rutherford et al. [60] did not measure the E_m precisely but concluded, in agreement with Shuvalov et al., that it is more negative than -0.60 V. We have therefore taken the E_m to be -0.62 V. Using -0.52 V instead of -0.62 V would lower the calculated free energies of all of the radical-pair states by 2.3 kcal/mol. It would not affect the calculated energy difference between $P^+B_L^-$ and $P^+H_L^-$, nor that between $P^+B_L^-$ and $P^+B_M^-$.

A difficulty inherent in comparing E_m values measured in the reaction center and in vitro is that an unknown junction potential is needed in order to connect measurements made in organic and aqueous solvents. This problem does not enter directly into any

of the present calculations. The calculation of the free energy of $P^+H_L^-$ is based on the difference between the E_m values of P and H_L in the reaction center. The free energy difference between $P^+B_L^-$ and $P^+H_L^-$ is calculated by using the difference between the E_m values of BChl and BPh in organic solvents.

(b) Errors resulting from using too restricted a region of the protein were evaluated by varying the model. Similar results for the free energies of the radical-pair states were obtained when the radius for trimming around each electron carrier was increased from 17 to 19 Å (Table II). In the calculations on P^+, we also obtained similar electrostatic energies after trimming the protein structure in rather different ways (Table III, structures A and B), provided that both structures occupied sufficiently large spheres around the BChls. Reducing the model to an extremely small set of amino acid residues of course can give very different results (Table III, structures C and D).

Another useful test of a model is whether similar values for ΔG_{elec} are obtained in calculations involving different paths of a thermodynamic cycle. In the present case, ΔG_{elec} for the reaction $P^+B_L^-H_L \rightarrow P^+B_LH_L^-$ was calculated both directly and by subtracting the values for the reactions $PB_L \rightarrow P^+B_L^-$ and $PH_L \rightarrow P^+H_L^-$ (Table II). The results, though not identical, agree reasonably well.

(c) The most important of the groups that are bound directly to the electron carriers are the histidine ligands of the four BChls. To examine the sensitivity of the results to the assumptions concerning these ligands, we treated the imidazole rings in two different ways. The two treatments differ in the way they deal with the changes in charge that occur on the imidazole rings in response to oxidation or reduction of the BChls. Treatment 1 depends on α to incorporate the effects of these changes; treatment 2 assumes that the effects can be included in ΔV_{ind}. Treatment 1 thus is strictly applicable only if the E_m values of the electron donor and acceptor can be measured in situ (as they can in the case of $P^+H_L^-$) or if the contributions of the ligands to the orbital energies are constant or are known. Treatment 2 is more widely applicable, but is clearly an approximation that needs scrutiny. Very different electrostatic energies and gas-phase energies are obtained in the two treatments, as is expected; but the final free energies are essentially the same (Tables I–V). This is partly a reflection of the reaction center's symmetry: the distances of the Mg atoms to the histidyl N_ϵ atoms are similar for the M and L pigments, so the contributions of the histidines to the orbital energies cannot be very different. The success of treatment 2 probably also reflects the fact that the Mg atom plays a relatively minor role in the π molecular orbitals that relinquish or gain an electron. In any event, the final uncertainties associated with the treatment of the histidines appear to be less than ± 1 kcal/mol. These uncertainties may be larger in calculations on the reaction center of *Rb. sphaeroides,* where the MgN_ϵ distances evidently vary substantially [6].

Hydrogen bonding also can affect the molecular orbital energies of the pigments, but these effects probably are reproduced reasonably well in the calculated electrostatic energies. For example, the carboxylic acid group of Glu-L104 was calculated to contribute about 1 kcal/mol to the free energy difference between $P^+H_L^-$ and $P^+B_L^-$ (Table II). This agrees well with molecular orbital calculations by Hanson et al. [77], which indicate that the hydrogen bonding of this group to H_L would change the reduction potential of the BPh by about 0.04 eV (0.9 kcal/mol).

(d) Structural distortions of the pigments could affect the molecular orbital energies so that the gas-phase energies for the electron transfer reactions in the reaction center differ from those of BChl and BPh in vitro. Barkigia et al. [76] have suggested that such distortions are important for fine-tuning the redox potentials of the pigments. This soure of error would not affect our calculation of the free energy of $P^+H_L^-$, which is based on E_m values measured in the reaction center. But it could affect the calculated freee energy difference between $P^+B_L^-$ and $P^+H_L^-$, as well as the differences between $P^+B_M^-$ and $P^+B_L^-$ and between $P^+H_M^-$ and $P^+H_L^-$. These errors are unlikely to be large, because the distortions of B_L, B_M, H_L and H_M from planarity appear to be minor.

(e) Uncertainties associated with the charges and polarizabilities assigned to the atoms were evaluated by comparing the results of using alternative parameters. Two different sets of atomic charges gave very similar results for the overall electrostatic energies and free energies. Two different treatments of the atomic polarizabilities also gave similar results (see Methods). In contrast, the individual terms that contribute to ΔG_{elec}, such as $\Delta V_{Q\mu}$, depend strongly on the parametrization of the atomic charges, so one should not attach much certainty to the absolute values of these terms (Tables II and III). The standard set of charges that we used in most of the calculations [49,50] are smaller for peptide C, O, N and H atoms than those of the alternative set [56], and are larger for side-chain aliphatic C and H atoms. There is little basis for choosing between the two sets of charges because both have been used in numerous molecular dynamics simulations of proteins and have given results that appear to be consistent with experiment. (See Ref. 78 for a recent example of simulations employing essentially the same set of charges as was used in most of the present work.)

Although errors could arise from neglecting the charges of ionized amino acid side chains, these errors are probably less than ± 1 kcal/mol. With the exception of Asp-L60, Arg-C15, Arg-L103 and Glu-L106, all

of the ionizable residues within 20 Å of B_L or H_L are likely to be in their neutral forms. The charges on these four residues were estimated to increase the free energy difference between $P^+B_L^-$ and $P^+H_L^-$ by about 0.5 kcal/mol. Similarly, Asp-L60 and Arg-C15 are probably the only charged residues that are close enough to affect the free energy difference between $P^+B_L^-$ and $P^+B_M^-$, and their charges were estimated to change the energy by only about 0.1 kcal/mol. Many of the more distant residues are likely to be charged, but these probably are well solvated so that their electrostatic interactions with the pigments are strongly screened.

An illustration of the screening of interactions between widely separated charged groups in the reaction center can be seen in the interactions of H_L and Q_A. Although the quinone ring of Q_A is centered only about 13 Å from the center of H_L, there is very little difference between the apparent free energies of the P^+I^- radical pair when the quinone is present in the form of the negatively charged Q_A^- radical and when the quinone is extracted from the reaction center [37,38]. Reduction of Q_A also has only a relatively small effect on the kinetics of electron transfer from P* to H_L [18]. This is in accord with discussions of the apparent dielectric constant for long-range charge–charge interactions in other proteins [48,52].

(f) The crystallographic coordinates used here have been refined at a resolution of 2.3 Å [3], which means that there could be errors on the order of ±0.2 Å in the positions of some of the atoms. The coordinates of the ring systems of the pigments are known with relatively high certainty; those of the phytol side-chains and some of the amino acid residues are less secure. The positions of all of the hydrogen atoms are intrinsically uncertain, because these atoms are not resolved in the crystal structure. We have not attempted to explore how changes in the coordinates might affect the calculated values of ΔG_{elec}, with the exception of the phenolic hydrogen atom of Tyr-M208. For most of the calculations, this atom was positioned so as to minimize the energy of its electrostatic interactions with the surroundings in the ground state. Rotating the phenolic OH bond by 40° in one direction about the C_ζ–O bond, which probably would constitute a relatively severe perturbation of the structure, increased the calculated free energy of $P^+B_L^-$ by 1.4 kcal/mol and the free energy difference between $P^+B_L^-$ and $P^+H_L^-$ by 0.5 kcal/mol. Rotating by 40° in the opposite direction had less effect: the calculated free energy of $P^+B_L^-$ increased by 0.4 kcal/mol and the free energy difference between $P^+B_L^-$ and $P^+H_L^-$ by 0.5 kcal/mol. Neither rotation had a significant effect on the calculated free energy of $P^+H_L^-$, because the small changes in ΔG_{elec} were balanced by changes in α. The calculations of λ should be insensitive to errors in the coordinates, because the structure is allowed to relax at each step in these calculations.

In general, it appears that the only way to check the accuracy of calculations on such a complicated system is to calculate a variety of properties that can be verified experimentally. The reaction center presents a special challenge because many of its radical-pair states may not even be detectable experimentally; measurements of their energies are uncertain if not impossible. However, the theoretical methods that we have used here have been applied successfully in other related problems, such as the calculation of electrostatic effects on the E_m of cytochrome *c* [51,52]. The results obtained in those systems are consistent with the conclusion that the overall error range of the present calculations is approx. ±2.5 kcal/mol. Although still larger than one would like, this represents a significant improvement on the uncertainties of ±5 kcal/mol in our previous calculations on the reaction center [31].

Implications of the calculated free energies for the electron transfer reactions

The calculated free energies of the radical-pairs states that we have considered are collected in Fig. 3. The relaxed $P^+H_L^-$ radical-pair is calculated to lie approx. 22.0 kcal/mol above the ground state, or 7.0 kcal/mol (0.30 eV) below P*. Considering the uncertainties in the calculations, the calculated free energy gap between P* and the relaxed radical-pair agrees well with the value of about 6.0 kcal/mol (0.26 eV) that has been obtained experimentally for the gap between P* and P^+I^- in *Rb. sphaeroides* reaction centers at room temperature [34,37–39,41,42]. However, the present calculations were done using the structure of the reaction center from *Rp. viridis,* and there is insufficient experimental information to allow such a comparison for this species. The substantially smaller free energy gap of about 2.0 kcal/mol (0.09 eV) between P* and the unrelaxed $P^+H_L^-$ radical-pair agrees with the time-resolved fluorescence measurements, which suggest that P^+I^- undergoes a series of relaxations on the time scale of 0 to 3 ns in both species [37–39].

The unrelaxed form of $P^+B_L^-$, whose energy cannot be measured experimentally, is calculated to lie about 2.0 kcal/mol above the unrelaxed $P^+H_L^-$, or very close to P*. This includes the estimated effects of the Fe and of the charged amino acid residues within 20 Å. The conclusion that $P^+B_L^-$ is approximately isoenergetic with P* would be consistent with the formation of the $P^+B_L^-$ radical-pair as a discrete intermediate in the electron transfer pathway. If the free energy gap between the two states is less than 1 or 2 kcal/mol, as the calculations suggest, the two-step mechanism through $P^+B_L^-$ is likely to predominate over the superexchange pathway, at least at room temperature [31]. The super-

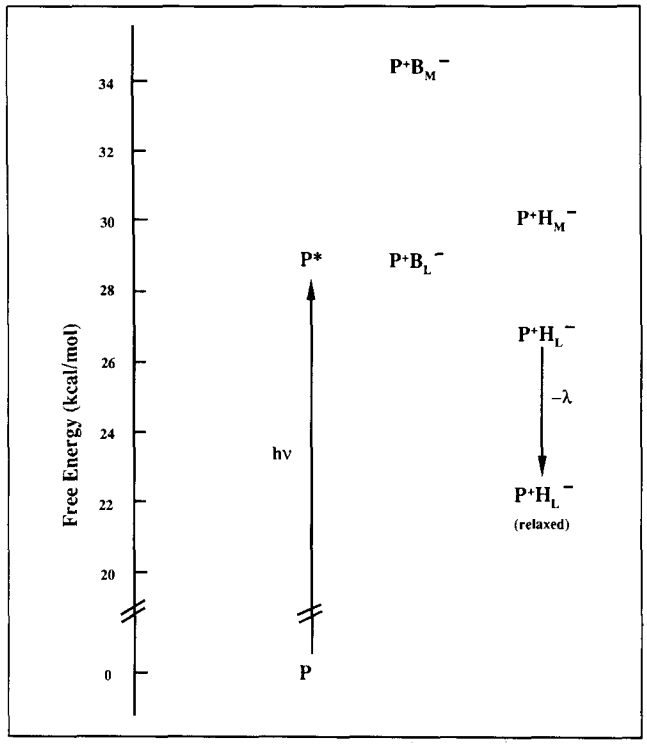

Fig. 3. Calculated standard free energies of radical-pair states and the lowest excited single state (P*) in the *Rp. viridis* reaction center. The free energy of P* is taken to the the mean of the absorption and emission maxima at 298 K. The free energies of the radical-pair states are for unrelaxed species in the ground-state geometry, with the exception of the $P^+H_L^-$ state labeled 'relaxed'; the free energy for this last state includes the calcualted reorganization energy ($\lambda_{P^+H^-}$). The estimated uncertainties of the calculated free energies are approx. ± 2.5 kcal/mol. The states represented here are adiabatic states.

exchange mechanism continues to be a viable alternative, however, because of the remaining uncertainty of about ± 2.5 kcal/mol in the calculated free energies.

The calculated free energies of all the radical-pair states would be increased slightly if we assumed that the positive charge of P^+ tends to localize on P_M, as is suggested by the calculations shown in Table III. In the models that are trimmed at 17 Å around the electron carriers, putting 70% of the charge on P_M raises the calculated energy of $P^+B_L^-$ by about 0.7 kcal/mol (Table IV). Putting 70% of the charge on P_L lowers the energy by 0.5 kcal/mol. As discussed above, EPR, ENDOR and TRIPLE resonance measurements are consistent with an asymmetric charge distribution, but do not indicate whether the larger charge is on P_L or on P_M. We therefore have not made this correction in Fig. 3.

Tyrosine M208 appears to play a particularly important role in lowering the energy of $P^+B_L^-$ (Table II). The tyrosine at this position is conserved in reaction centers from *Rhodopseudomonas viridis, Rhodobacter sphaeroides, Rhodobacter capsulatus* and *Rhodospirillum rubrum,* but is replaced by leucine in *Chloroflexus aurantiacus* [10]. The homologous residue on the M side is phenylalanine in all cases [10,79]. If the present calculations are correct, it should be possible to raise the energy of $P^+B_L^-$ above that of P* by genetic modifications at this site, for example by replacing the tyrosine with phenylalanine. The rate of formation of the radical-pair should decrease significantly once the energy gap between the two states becomes greater than the thermal fluctuations in the energies. The initial electron transfer reaction is slower in *Cf. aurantiacus* than it is in *Rp. viridis, Rb. sphaeroides* or *Rb. capsulatus* [80], but whether this is related to the replacement of the tyrosine by leucine cannot be determined at present because the reaction centers differ at other sites as well.

Bixon et al. [43,81] have concluded that $P^+B_L^-$ must be at least 5 kcal/mol above $P^+H_L^-$ in order to be consistent with the temperature independence of the exchange interaction between P^+ and I^-. It is difficult to relate this conclusion directly to our results because the thermally equilibrated form of $P^+B_L^-$ that might contribute to the exchange interaction is not the same as the unrelaxed species we have considered. The reorganization energy of $P^+B_L^-$ is likely to be somewhat smaller than the λ of 5.0 kcal/mol that we calculated for $P^+H_L^-$. However, if we estimate the reorganization energy of $P^+B_L^-$ to be 4.0 kcal/mol, the relaxed $P^+B_L^-$ would be about 3 kcal/mol above $P^+H_L^-$, which is smaller than the lower limit set by Bixon et al. We cannot offer a fully satisfactory explanation for this discrepancy. As Won and Friesner [82] have pointed out, however, the matrix elements that govern the exchange interaction in P^+I^- may be difficult to evaluate because they depend on the complex mixture of basis states that make up P*.

The unrelaxed $P^+B_M^-$ radical-pair was calculated to lie about 5.5 kcal/mol above $P^+B_L^-$ and P*. If this result is correct, $P^+B_M^-$ could not be formed without the aid of thermal activation. The activation energy seems sufficiently large to explain why electron transfer in the M direction does not compete significantly with the formation of $P^+H_L^-$. At cryogenic temperatures, where the experimental evidence for the specificity of the reaction is best, the rate of formation of $P^+H_L^-$ would be very low by either the two-step mechanism or superexchange.

The higher eigenstates of $P^+B_L^-$ and $P^+H_L^-$ also appear to be too high in energy to participate significantly in the electron transfer mechanism. But one probably should not dismiss such a participation altogether, because the energy splitting between the two forms of $P^+B_L^-$ or $P^+H_L^-$ depends largely on the resonance interaction matrix element U_{LM}, which cannot be measured experimentally. In principle, the existence of a manifold of $P^+B_L^-$ states extending both above and below P* could help to make the reaction insensitive to

temperature or minor structural perturbations. If one of the antisymmetric radical pairs did form in an initial electron-transfer step, it probably would decay extremely rapidly to the lower-lying symmetric species. This might provide a partial answer to the question of why photosynthetic organisms use a dimer for the primary electron donor. It might be possible to test the calculations of the separation between the higher and lower eigenstates of P^+ by locating the absorption band that should result from transitions between these two states. The present calculations suggest that this band might be seen in the infrared spectrum in the region of 5 μm.

Appendix

Atomic charges for BChl b and BPh b and their radicals

Atom	BChl	$BChl^+$	$BChl^-$	BPh	BPh^-
CHB	−0.016	0.020	−0.070	0.019	−0.016
HCHB	0.000	0.000	0.000	0.000	0.000
C1B	−0.008	0.078	−0.049	0.078	−0.008
C2B	−0.041	−0.001	−0.093	−0.001	−0.041
CMB	−0.291	−0.291	−0.291	−0.291	−0.291
HMB1	0.097	0.097	0.097	0.097	0.097
HMB2	0.079	0.097	0.097	0.097	0.097
HMB3	0.097	0.097	0.097	0.097	0.097
C3B	−0.044	−0.012	−0.090	−0.012	−0.044
CAB	0.220	0.220	0.201	0.220	0.220
CBB	−0.291	−0.291	−0.291	−0.291	−0.291
HBB1	0.097	0.097	0.097	0.097	0.097
HBB2	0.097	0.097	0.097	0.097	0.097
HBB3	0.097	0.097	0.097	0.097	0.097
OBB	−0.287	−0.277	−0.314	−0.287	−0.287
C4B	−0.019	0.101	−0.051	0.101	−0.019
NB	−0.208	−0.198	−0.209	−0.194	−0.208
CHC	0.017	0.015	−0.063	0.019	0.017
HCHC	0.000	0.000	0.000	0.000	0.000
C1C	−0.024	0.052	−0.037	0.052	−0.024
C2C	−0.097	−0.097	−0.097	−0.097	−0.097
HC2C	0.097	0.097	0.097	0.097	0.097
CMC	−0.291	−0.291	−0.291	−0.291	−0.291
HMC1	0.097	0.097	0.097	0.097	0.097
HMC2	0.097	0.097	0.097	0.097	0.097
HMC3	0.097	0.097	0.097	0.097	0.097
C3C	0.000	0.000	0.000	0.000	0.000
CAC	−0.097	−0.097	−0.097	−0.097	−0.097
HAC	0.097	0.097	0.097	0.097	0.097
CBC	−0.291	−0.291	−0.291	−0.291	−0.291
HBC1	0.097	0.097	0.097	0.097	0.097
HBC2	0.097	0.097	0.097	0.097	0.097
HBC3	0.097	0.097	0.097	0.097	0.097
C4C	−0.023	0.097	−0.064	0.097	−0.023
NC	−0.054	−0.040	−0.126	−0.041	−0.054
CHD	0.010	0.040	−0.068	0.040	0.010
HCHD	0.000	0.000	0.000	0.000	0.000
C1D	−0.008	0.062	−0.056	0.062	−0.008
C2D	−0.009	0.025	−0.072	0.026	−0.009
CMD	−0.291	−0.291	−0.291	−0.291	−0.291
HMD1	0.097	0.097	0.097	0.097	0.097
HMD2	0.097	0.097	0.097	0.097	0.097
HMD3	0.097	0.097	0.097	0.097	0.097
C3D	−0.047	−0.027	−0.094	−0.027	−0.047
CAD	0.213	0.213	0.206	0.213	0.213
OBD	−0.269	−0.263	−0.284	−0.264	−0.269
CBD	−0.097	−0.097	−0.097	−0.097	−0.097
HCBD	0.097	0.097	0.097	0.097	0.097
CGD	0.700	0.700	0.700	0.700	0.700
O1D	−0.350	−0.350	−0.350	−0.350	−0.350
O2D	−0.350	−0.350	−0.350	−0.350	−0.350
CED	−0.291	−0.291	−0.291	−0.291	−0.291
HED1	0.097	0.097	0.097	0.097	0.097
HED2	0.097	0.097	0.097	0.097	0.097
HED3	0.097	0.097	0.097	0.097	0.097
C4D	0.007	0.101	−0.048	0.101	0.007
ND	−0.224	−0.212	−0.234	−0.207	−0.224
CHA	−0.072	−0.066	−0.137	−0.066	−0.072
C1A	0.008	0.064	−0.004	0.065	0.008
C2A	−0.097	−0.097	−0.097	−0.097	−0.097
HC2A	0.097	0.097	0.097	0.097	0.097
CAA	−0.194	−0.194	−0.194	−0.194	−0.194
HAA1	0.097	0.097	0.097	0.097	0.097
HAA2	0.097	0.097	0.097	0.097	0.097
CBA	−0.194	−0.194	−0.194	−0.194	−0.194
HBA1	0.097	0.097	0.097	0.097	0.097
HBA2	0.097	0.097	0.097	0.097	0.097
CGA	0.700	0.700	0.700	0.700	0.700
O1A	−0.350	−0.350	−0.350	−0.350	−0.350
O2A	−0.350	−0.350	−0.350	−0.350	−0.350
C3A	−0.097	−0.097	−0.097	−0.097	−0.097
HC3A	0.097	0.097	0.097	0.097	0.097
CMA	−0.291	−0.291	−0.291	−0.291	−0.291
HMA1	0.097	0.097	0.097	0.097	0.097
HMA2	0.097	0.097	0.097	0.097	0.097
HMA3	0.097	0.097	0.097	0.097	0.097
C4A	−0.022	0.086	−0.042	0.086	−0.022
NA	−0.101	−0.081	−0.202	−0.080	−0.100
MG	1.001	1.003	1.000	–	–
HNB	–	–	–	0.000	0.000
HND	–	–	–	0.000	0.000

Acknowledgements

We thank the National Science Foundation (grant PCM-8616161) and the National Institutes of Health (GM-40283) for support and Dr. J. Deisenhofer for providing the crystallographic coordinates.

References

1 Deisenhofer, J., Epp, O., Miki, K., Huber, R. and Michel, H. (1985) Nature 318, 618–624.
2 Michel, H., Epp, O. and Deisenhofer, J. (1986) EMBO J. 5, 2445–2451.
3 Deisenhofer, J. and Michel, H. (1988) in The Photosynthetic Bacterial Reaction Center. Structure and Dynamics (Breton, J., and Verméglio, A., eds.), pp. 1–3, Plenum, New York.
4 Chang, D.-H., Tiede, D., Tang, J., Smith, U., Norris, J. and Schiffer, M. (1986) FEBS Lett. 205, 82–86.
5 Allen, J.P., Feher, G., Yeates, T.O., Komiya, H. and Rees, D.C. (1987) Proc. Natl. Acad. Sci. USA 84, 6162–6166.

6 Yeates, T.O., Komiya, H., Chirino, A., Rees, D.C., Allen, J.P. and Feher, G. (1988) Proc. Natl. Acad. Sci. USA 85, 7993–7997.
7 Youvan, D.C., Bylina, E.J., Alberti, M., Megush, H. and Hearst, J. (1985) Cell 37, 949–957.
8 Williams, J.C., Steiner, L.A., Feher, G. and Simon, M. (1984) Proc. Natl. Acad. Sci. USA 81, 7303–7307.
9 Michel, H., Weyer, K.A., Gruenberg, H., Dunger, I., Oesterhelt, D. and Lottspeich, F. (1986) EMBO J. 5, 1149–1158.
10 Komiya, H., Yeates, T.O., Rees, D.C., Allen, J.P. and Feher, G. (1988) Proc. Natl. Acad. Sci. USA 85, 9012–9016.
11 Parson, W.W., Clayton, R.K. and Cogdell, R.J. (1975) Biochim. Biophys. Acta 387, 265–278.
12 Rockley, M., Windsor, M.W., Cogdell, R.J. and Parson, W.W. (1975) Proc. Natl. Acad. Sci. USA 72, 2251–2255.
13 Kirmaier, C., Holten, D. and Parson, W.W. (1985) Biochim. Biophys. Acta 810, 33–48.
14 Kirmaier, C., Holten, D. and Parson, W.W. (1985) Biochim. Biophys. Acta 810, 49–61.
15 Bylina, E.J., Kirmaier, C., Mc Dowell, L., Holten, D. and Youvan, D.C. (1988) Nature 336, 182–184.
16 Michel-Beyerle, M.E., Plato, M., Deisenhofer, J., Michel, H., Bixon, M. and Jortner, J. (1988) Biochim. Biophys. Acta 932, 52–70.
17 Holten, D., Hoganson, C., Windsor, M.W., Schenck, C.C., Parson, W.W., Migus, A., Fork, R.L. and Shank, C.V. (1980) Biochim. Biophys. Acta 592, 461–477.
18 Woodbury, N.W., Becker, M., Middendorf, D. and Parson, W.W. (1985) Biochemistry 24, 7516–7521.
19 Paschenko, V.Z., Korvatovskii, B.N., Kononenko, A.A., Chamorovsky, S.K. and Rubin, A.B. (1985) FEBS Lett. 191, 245–248.
20 Martin, J.-L., Breton, J., Hoff, A.J., Migus, A. and Antonetti, A. (1986) Proc. Natl. Acad. Sci. USA 83, 957–961.
21 Breton, J., Martin, J.-L., Migus, A., Antonetti, A. and Orszag, A. (1986) Proc. Natl. Acad. Sci. USA 83, 5121–5125.
22 Wasielewski, M.R. and Tiede, D.M. (1986) FEBS Lett. 204, 368–372.
23 Kirmaier, C. and Holten, D. (1988) Israel J. Chem. 28, 79–85.
24 Robert, B., Lutz, M. and Tiede, D.M. (1985) FEBS Lett. 183, 326–330.
25 Shuvalov, V.A., Klevanik, A.V., Sharkov, A.V., Matveetz, Ju.A. and Krukov, P.G. (1978) FEBS Lett. 91, 135–139.
26 Shuvalov, V.A. and Klevanik, A.V. (1983) FEBS Lett. 160, 51–55.
27 Kirmaier, C., Holten, D. and Parson, W.W. (1985) FEBS Lett. 185, 76–81.
28 Breton, J., Martin, J.-L., Petrich, J., Migus, A. and Antonetti, A. (1986) FEBS Lett. 209, 37–43.
29 Fleming, G.R., Martin, J.-L. and Breton, J. (1988) Nature 33, 190–192.
30 Holzapfel, W., Finkele, U., Kaiser, W., Oesterhelt, D., Scheer, H., Stilz, H.U. and Zinth, W. (1989) Chem. Phys. Lett. 160, 1–7.
31 Creighton, S., Hwang, J.-K., Warshel, A., Parson, W.W. and Norris, J.R. (1988) Biochemistry 27, 774–781.
32 Marcus, R. (1988) Israel, J. Chem. 28, 205–213.
33 Schenck, C.C., Blankenship, R.E. and Parson, W.W. (1982) Biochim. Biophys. Acta 680, 44–59.
34 Ogrodnik, A., Volk, M., Letterer, R., Feick, R. and Michel-Beyerle, M.E. (1988) Biochim. Biophys. Acta 936, 361–371.
35 Werner, H.-J., Schulten, K. and Weller, A. (1978) Biochim. Biophys. Acta 502, 255–268.
36 Haberkorn, R. and michel-Beyerle, M.E. (1979) Biophys. J. 26, 489–498.
37 Woodbury, N.W.T. and Parson, W.W. (1984) Biochim. Biophys. Acta 767, 345–361.
38 Woodbury, N.W., Parson, W.W., Gunner, M.R., Prince, R.C. and Dutton, P.L. (1986) Biochim. Biophys. Acta 851, 6–22.
39 Hörber, J.K.H., Göbel, W., Ogrodnik, A., Michel-Beyerle, M.E. and Cogdell, R.J. (1986) FEBS Lett. 198, 273–278.
40 Chidsey, C.E.D., Takiff, L., Goldstein, R.A. and Boxer, S.G. (1985) Proc. Natl. Acad. Sci. USA 82, 6850–6854.
41 Goldstein, R.A., Takiff, L. and Boxer, S.G. (1988) Biochim. Biophys. Acta 934, 253–263.
42 Goldstein, R.A. and Boxer, S. (1989) Biochim. Biophys. Acta 977, 78–86.
43 Bixon, M., Jortner, J., Michel-Beyerle, M.E., Ogrodnik, A. and Lersch, W. (1987) Chem. Phys. Lett. 140, 626–630.
44 Hunter, D.A., Hoff, A.J. and Hore, P.J. (1987) Chem. Phys. Lett. 134, 6–11.
45 Ogrodnik, A., Remy-Richter, N., Michel-Beyerle, M.E. and Feick, R. (1987) Chem. Phys. Lett. 135, 576–581.
46 Warshel, A., Chu, Z.T. and Parson, W.W. (1989) Science 246, 112–116.
47 Parson, W.W., Creighton, S. and Warshel, A. (1989) J. Am. Chem. Soc. 111, 4277–4284.
48 Warshel, A. and Russell, S. (1984) Quart. Rev. Biophys. 17, 283–422.
49 Russell, S. and Warshel, A. (1985) J. Mol. Biol. 185, 389–404.
50 Warshel, A. and Russell, S. (1986) J. Am. Chem. Soc. 108, 6569–6579.
51 Warshel, A., Sussman, F. and King, G. (1986) Biochemistry 25, 8368–8372.
52 Cutler, R.L., Davies, A.M., Creighton, S., Warshel, A., Moore, G.R., Smith, M. and Mauk, A.G. (1989) Biochem. 28, 3188–3197.
53 Warshel, A. and Creighton, S. (1989) in Computer Simulations of Biomolecular Systems (Van Gunsteren, W.F. and Weiner, P.K., eds.), pp. 120–138, ESCOM Science Publishers, Leiden.
54 Warshel, A. and Lappicerella, A. (1981) J. Am. Chem. Soc. 103, 4664–4673.
55 Weiner, S.J., Kollman, P.A., Nguyen, D.T. and Case, D.A. (1986) J. Comp. Chem. 7, 230–252.
56 Yeates, T.O., Komiya, H., Rees, D.C., Allen, J.P. and Feher, G. (1987) Proc. Natl. Acad. Sci. USA 84, 6438–6442.
57 Carithers, R.P. and Parson, W.W. (1975) Biochim. Biophys. Acta 387, 194–211.
58 Shuvalov, V.A., Krakhmaleva, I.N. and Klimov, V.V. (1976) Biochim. Biophys. Acta 449, 597–601.
59 Prince, R.C., Leigh, J.S. and Dutton, P.L. (1976) Biochim. Biophys. Acta 440, 622–636.
60 Rutherford, A.W., Heathcote, P. and Evans, M.C.W. (1979) Biochem. J. 182, 515–523.
61 Shopes, R.J. and Wraight, C.A. (1987) Biochim. Biophys. Acta 893, 409–425.
62 Warshel, A. (1982) J. Phys. Chem. 86, 2218–2224.
63 Fajer, J., Borg, D.C., Forman, A., Dolphin, D. and Felton, R.H. (1973) J. Am. Chem. Soc. 95, 2739–2740.
64 Fajer, J., Borg, D.C., Forman, A., Felton, R., Dolphin, D. and Vegh, L. (1974) Proc. Natl. Acad. Sci. USA 71, 994–998.
65 Fajer, J., Davis, M.S., Brune, D.C., Spaulding, L.D., Borg, D.C. and Forman, A. (1976) Brookhaven. Symp. Biol. 28, 183–103.
66 Warshel, A. and Parson, W.W. (1987) J. Am. Chem. Soc. 109, 6143–6152.
67 Parson, W.W. and Warshel, A. (1987) J. Am. Chem. Soc. 109, 6152–6163.
68 Warshel, A., Creighton, S. and Parson, W.W. (1988) J. Phys. Chem. 92, 2696–2701.
69 Treutlein, H., Schulten, K., Niedermeier, C., Deisenhofer, J., Michel, H. and DeVault, D. (1988) in The Photosynthetic Bacterial Reaction Center. Structure and Dynamics (Breton, J., and Verméglio, A., eds.), pp. 369–377, Plenum, New York.
70 Davis, M.S., Forman, A., Hanson, L.K., Thornber, J.P. and Fajer, J. (1979) J. Phys. Chem. 83, 3325–3332.
71 Lubitz, W., Lendzian, F., Plato, M., Möbius, K. and Tränkle, E.

(1985) in Antennas and Reaction Centers of Photosynthetic Bacteria – Structure, Interactions and Dynamics (Michel-Beyerle, M.E., ed.), pp. 164–173, Springer, Berlin.
72 Plato, M., Lendzian, F., Lubitz, W., Tränkle, E. and Möbius, K. (1988) in The Photosynthetic Bacterial Reaction Center. Structure and Dynamics (Breton, J. and Verméglio, A., eds.), pp. 379–388, Plenum, New York.
73 Lendzian, F., Lubitz, W., Scheer, H., Hoff, A.J., Plato, M., Tränkle, E. and Möbius, K. (1988) Chem. Phys. Lett. 148, 377–385.
74 Plato, M., Lubitz, W., Lendzian, F., Tränkle, E. and Möbius, K. (1988) Isr. J. Chem. 28, 109–119.
75 Plato, M., Möbius, K., Michel-Beyerle, M.E., Bixon, M. and Jortner, J. (1988) J. Am. Chem. Soc. 110, 7279–7285.
76 Barkigia, K.M., Chantranupong, L., Smith, K.M. and Fajer, J. (1988) J. Am. Chem. Soc. 110, 7566–7567.
77 Hanson, L.K., Thompson, M.A., Zerner, M.C. and Fajer, J. (1988) in The Photosynthetic Bacterial Reaction Center. Structure and Dynamics (Breton, J. and Verméglio, A., eds.), pp. 355–367, Plenum, New York.
78 Levitt, M. and Sharon, R. (1988) Proc. Natl. Acad. Sci. USA 85, 7557–7561.
79 Tiede, D.M., Budil, D.E., Tang, J., El-Kabbani, O., Norris, J.R., Chang, C.-H. and Schiffer, M. (1988) in The Photosynthetic Bacterial Reaction Center. Structure and Dynamics (Breton, J. and Verméglio, A., eds.), pp. 13–20, Plenum, New York.
80 Becker, M., Middendorf, D., Woodbury, N.W., Parson, W.W. and Blankenship, R.E. (1986) in Ultrafast Phenomena, V (Fleming, G.R. and Siegman, A.E., eds.), pp. 374–378, Springer, New York.
81 Bixon, M., Michel-Beyerle, M.E. and Jortner, J. (1988) Isr. J. Chem. 28, 155–168.
82 Won, Y. and Friesner, R.A. (1988) Biochim. Biophys. Acta 935, 9–18.
83 Roth, M., Lewit-Bentley, A., Michel, H. and Deisenhofer, J. (1989) Nature 340, 659–661.
84 Connolly, J.S., Samuel, E.B. and Janzen, A.F. (1982) Photochem. Photobiol. 36, 565–574.